

# $^1\text{H}$ and $^{13}\text{C}$ NMR spectroscopic studies of the ferriheme resonances of three low-spin complexes of wild-type nitrophorin 2 and nitrophorin 2(V24E) as a function of pH

Fei Yang · Markus Knipp · Tatiana K. Shokhireva · Robert E. Berry · Hongjun Zhang · F. Ann Walker

Received: 16 March 2009 / Accepted: 24 May 2009 / Published online: 11 June 2009  
© SBIC 2009

**Abstract** The ferriheme resonances of the low-spin ( $S = 1/2$ ) complexes of wild-type (wt) nitrophorin 2 (NP2) and its heme pocket mutant NP2(V24E) with imidazole (ImH), histamine (Hm), and cyanide ( $\text{CN}^-$ ) as the sixth ligand have been investigated by NMR spectroscopy as a function of pH (4.0–7.5). For the three wt NP2 complexes, the ratio of the two possible heme orientational isomers, **A** and **B**, remains almost unchanged (ratio of **A**:**B** approximately 1:6 to 1:5) over this wide pH range. However, strong chemical exchange cross peaks appear in the nuclear Overhauser effect spectroscopy/exchange spectroscopy (NOESY/EXSY) spectra for the heme methyl resonances at low pH (pH\* 4.0–5.5), which indicate chemical exchange between two species. We have shown these to be two different exogenous ImH or Hm orientations that are denoted **B** and **B'**, with the ImH plane nearly parallel and perpendicular to the ImH plane of the protein-provided His57, respectively. The wt NP2–CN complex also shows EXSY cross peaks due to chemical exchange, which is shown to be a result of interchange between two ruffling distortions of the heme.

The same ruffling distortion interchange is also responsible for the ImH and Hm chemical exchange. For the three NP2(V24E) ligand complexes, no EXSY cross peaks are observed, but the **A**:**B** ratios change dramatically with pH. The fact that heme favors the **A** orientation highly for NP2(V24E) at low pH as compared with wt NP2 is believed to be due to the steric effect of the V24E mutation. The existence of the **B'** species at lower pH for wt NP2 complexes and the increase in **A** heme orientation at lower pH for NP2(V24E) are believed to be a result of a change in structure near Glu53 when it is protonated at low pH.  $^1\text{H}\{^{13}\text{C}\}$  heteronuclear multiple quantum coherence (HMQC) spectra are very helpful for the assignment of heme and nearby protein side chain resonances.

**Keywords** Nitrophorin · NMR · Ferriheme · Glutamate mutant · Imidazole complex

## Introduction

The nitrophorins (NPs) are a group of NO-carrying ferriheme proteins found in the saliva of the blood-sucking insect *Rhodnius prolixus*. At least five NPs, i.e., NP1, NP2, NP3, NP4, and NP7, are expressed in varying amounts during the six developmental stages of the insect's life cycle [1, 2]. The proteins are expressed in the endothelial cells of the salivary glands and, upon export and insertion of the heme *b* cofactor, a nitric oxide synthase in the gland endothelium is turned on and charges the distal Fe(III) coordination site of the NP with NO [3–5]. The Fe(III)–NO complex is very stable at the low pH of the saliva (pH 5–6), so NO can be stored for a long period of time [1, 6]. But upon injection of the NP–NO complexes into the tissues of the victim, NO dissociates from the NPs as a consequence

**Electronic supplementary material** The online version of this article (doi:10.1007/s00775-009-0551-3) contains supplementary material, which is available to authorized users.

F. Yang · T. K. Shokhireva · R. E. Berry · H. Zhang · F. A. Walker (✉)  
Department of Chemistry and Biochemistry,  
University of Arizona,  
1306 East University Boulevard,  
Tucson, AZ 85721-0041, USA  
e-mail: awalker@email.arizona.edu; awalker@u.arizona.edu

M. Knipp  
Max-Planck-Institut für Bioorganische Chemie,  
Stiftstraße 34-36,  
45470 Mülheim, Germany

of pH increase and dilution, thus causing vasodilation and inhibition of platelet aggregation. Meanwhile, the vacant sixth coordination site of the ferriheme center can capture histamine (Hm), which is released from mast cells and platelets of the victim. This results in a delay in the victim's immune response [7]. Both the NO release and the Hm trapping benefit the feeding of the insect.

To study the structures and unique properties of each NP, a number of spectroscopic and other techniques have been used, including spectroelectrochemistry [8–12], infrared [8], resonance Raman [13], NMR [8, 10, 14–20], EPR [8, 21], and Mössbauer [22] spectroscopies, stopped-flow photometry [9, 19, 23], and X-ray crystallography of one or more ligand complexes of NP1 [8, 24], NP2 [25, 26], and NP4 [27–31]. Compared with other heme proteins, NPs are unique with respect to the heme being located inside the open end of a  $\beta$ -barrel [32], rather than in the more commonly observed, largely  $\alpha$ -helical globin or four-helix bundle folds. The heme is bound to the NP via a His ligand, and the sixth coordination site is able to bind H<sub>2</sub>O, NO, Hm, or other ligands.

NMR is a very powerful spectroscopic technique for studying paramagnetic heme proteins, because the unpaired electrons on the Fe(III) center act as “beacons” that “illuminate” the protons nearby by causing isotropic shifts (also called “hyperfine shifts” or “paramagnetic shifts”) of the resonances from those observed in a diamagnetic protein [33–35]. These shifts are very useful for studying the electron configuration at the Fe center, the structure of the heme center, and its relationship to the protein matrix [33–35]. Once the assignment of the heme methyl resonances is available, the orientation of the nodal plane of the axial His imidazole with respect to the heme N–Fe–N axes can be derived [14]. The NO-free form of the NPs is high-spin ( $S = 5/2$ ), while upon binding to even-electron strong-field donor ligands such as imidazole (ImH), Hm, or cyanide it becomes low-spin ( $S = 1/2$ ). Since the NP–NO complexes are diamagnetic, cyanide ion has been used as an even-electron donor ligand model for NO [17] to fully utilize the paramagnetic shift information.

NP7 is a newly discovered NP, whose gene was found in the complementary DNA (cDNA) of fifth instar nymphs [36]. We have inserted this gene into a plasmid and expressed it in *Escherichia coli* (*E. coli*), and purified it from solubilized inclusion bodies [37]. In our previous study of NP7 [38, 39], NP2 and NP2(V24E) were chosen as models to better understand NP7, which has the unfortunate property of aggregating at the concentrations required for solution NMR experiments. NP7 was compared with NP2 because it shares an amino acid sequence identity of 61% and high-resolution X-ray structures of NP2 are available [25, 26], which allowed the calculation of a reliable homology model by using PDB files 1T68, 1PEE,

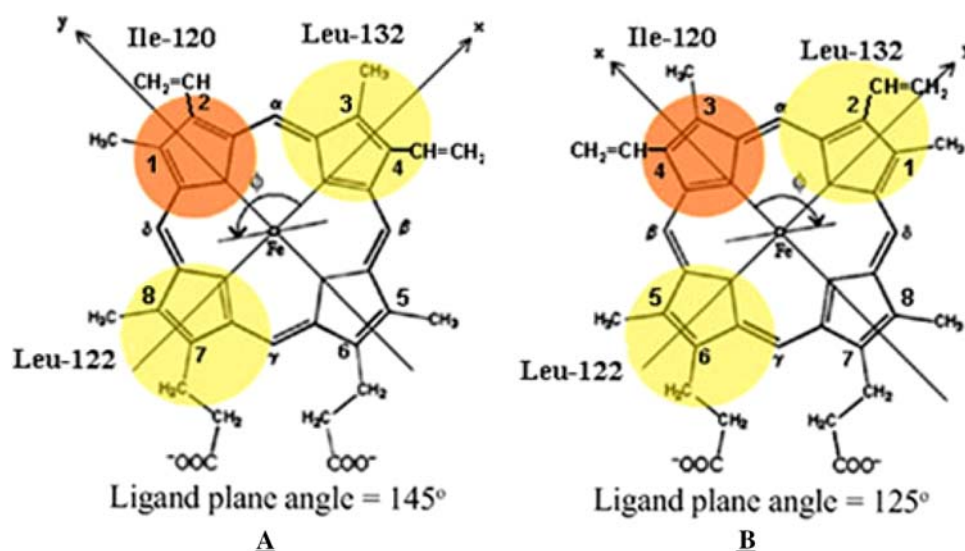
1EUO, and 2A3F as templates [38]. In contrast, for NP3, which shares an amino acid sequence identity of 62% with NP7, no X-ray structure is yet available. Among all the NMR investigations of NP1, NP2, NP3, and NP4 [11, 15–19], it has been found that NP2 has the simplest NMR spectra, because it exhibits one major heme orientation (Fig. 1) and no chemical exchange cross peaks [11, 15–17]. In addition, NP7 contains a unique carboxyl side chain residue, Glu27, which is close to pyrrole rings I and II of the heme. This residue is a Val in NP1, NP2, NP3, and NP4 (Val24 in NP2). To understand the specific impact of this carboxyl side chain on the properties of the protein, a site-specific mutant NP2(V24E) was generated and investigated. Unfortunately, the NP7 <sup>1</sup>H NMR spectra were extremely broad and difficult to assign at pH\* 7.0 [39], the pH that has been used until now for NMR studies of the NPs. However, we found that it could be studied at low pH (5.5) [39], which is, in fact, close to the pH of the salivary glands of the insect (between 5 and 6) [40]. We also had not investigated the NMR spectra of wild-type NP2 (wt NP2) at the low pH of the salivary glands. Thus, in this work we have studied NP2 and its V24E mutant at low pH to obtain a better understanding of NP7 at the pH of the salivary glands. Interestingly, we found that the spectra of NP2 were different at low pH from those studied earlier at pH\* 7.0 [15–17]. To explore these differences in greater detail, in this work we have studied the ImH, Hm, and cyanide complexes of not only wt NP2, but also its V24E mutant, by NMR spectroscopy to understand the pH dependence of the spectra. In the process we found and fully investigated both the chemical exchange process and changes in the heme A:B ratio (Fig. 1) with changes in pH.

## Materials and methods

### Preparation of recombinant proteins and buffers

Prior to protein expression, the previously described plasmids [19, 39] were transformed into *E. coli* strain BL21(DE3) (Novagen). NP2 and NP2(V24E) were expressed as inclusion bodies and purified as described previously for NP2 [23] and NP7 [37], respectively. The protein preparation involves the refolding and subsequent insertion of the cofactor. The yield of NP2(V24E) is very low and titration of hemin into the apoprotein is a long process because hemin not immediately incorporated into the protein precipitates. Stocks of NP2(V24E) were stored at  $-20\text{ }^{\circ}\text{C}$  in 100 mM NaOAc/HOAc, 10% (v/v) glycerol (pH 5.0) until use and wt NP2 was kept lyophilized at  $-20\text{ }^{\circ}\text{C}$ . D<sub>2</sub>O (99.9% deuterated) and acetic-*d*<sub>4</sub> acid (99.5% deuterated) were obtained from Cambridge Isotope Laboratories. ImH, Hm, sodium cyanide, and all other

**Fig. 1** Heme orientations **A** and **B**, with His57 behind the heme, and Ile120, Leu122, and Leu132 in front of the heme



chemicals used were of the highest quality available. The D<sub>2</sub>O buffer solutions, phosphate buffer, for instance, were initially prepared in H<sub>2</sub>O, including the adjustment of pH. After lyophilization, the solids were redissolved in D<sub>2</sub>O. The lyophilization/dissolution process was repeated at least three times before the solutions were used for NMR sample preparation. The pH of the buffers is not corrected for the deuterium isotope effect and, therefore, is designated pH\*.

#### NMR sample preparation and NMR data collection

NP2(V24E) samples were concentrated using Ultrafree ultrafiltration concentrators (NMWL 10 kDa) (Millipore). Buffer was exchanged through extensive washing (more than three times) with 30 mM sodium phosphate/acetic-*d*<sub>4</sub> acid buffer in D<sub>2</sub>O. wt NP2 samples were prepared from lyophilisates, as has been previously described [15]. NMR samples finally consisted of 1–2 mM solutions of each of the proteins. For the low-pH\* samples, pH\* was then adjusted through titration with acetic-*d*<sub>4</sub> acid using a standard pH electrode with H<sub>2</sub>O solution inside the glass electrode.

To obtain the low-spin complexes, the high-spin samples were titrated with the desired ligand (ImH, Hm, CN<sup>-</sup> in buffer at the chosen pH\*) until the proton NMR signals in the 70–30 ppm region, indicative of the high-spin form, had just disappeared. Concomitantly, these signals were replaced by much sharper signals in the 30–10 ppm region. In the case of CN<sup>-</sup>, the highest concentration of NaCN used at low pH\* was 2 mM, because of the tendency of excess CN<sup>-</sup> to replace His57; thus at low pH\* (5.5, 4.5) some evidence of high-spin Fe(III) resonances was apparent.

NMR data were collected over the temperature range of 10–37 °C with the chemical shifts referenced to residual protonated water using Bruker DRX-500 and DRX-600

NMR spectrometers, operating at 499.58- and 600.13-MHz <sup>1</sup>H Larmor frequencies, respectively. The <sup>1</sup>H{<sup>13</sup>C}-HMQC experiments were performed at 500 MHz using the 5-mm inverse-detection broadband probe with decoupling during acquisition. A recycle time of 250 ms and a refocusing time of 2.5 ms (*J* = 200 Hz) were used. The water-eliminated Fourier transform (WEFT) nuclear Overhauser effect spectroscopy (NOESY) experiment utilized 160 ms relaxation delay and 140–200 ms recovery-delay. The mixing times for the WEFT-NOESY experiments were 25–40 ms. All 2D spectra were collected with 1,024–2,048 data points in *t*<sub>2</sub> and with 200–500 blocks in *t*<sub>1</sub> with 512–650 scans per block.

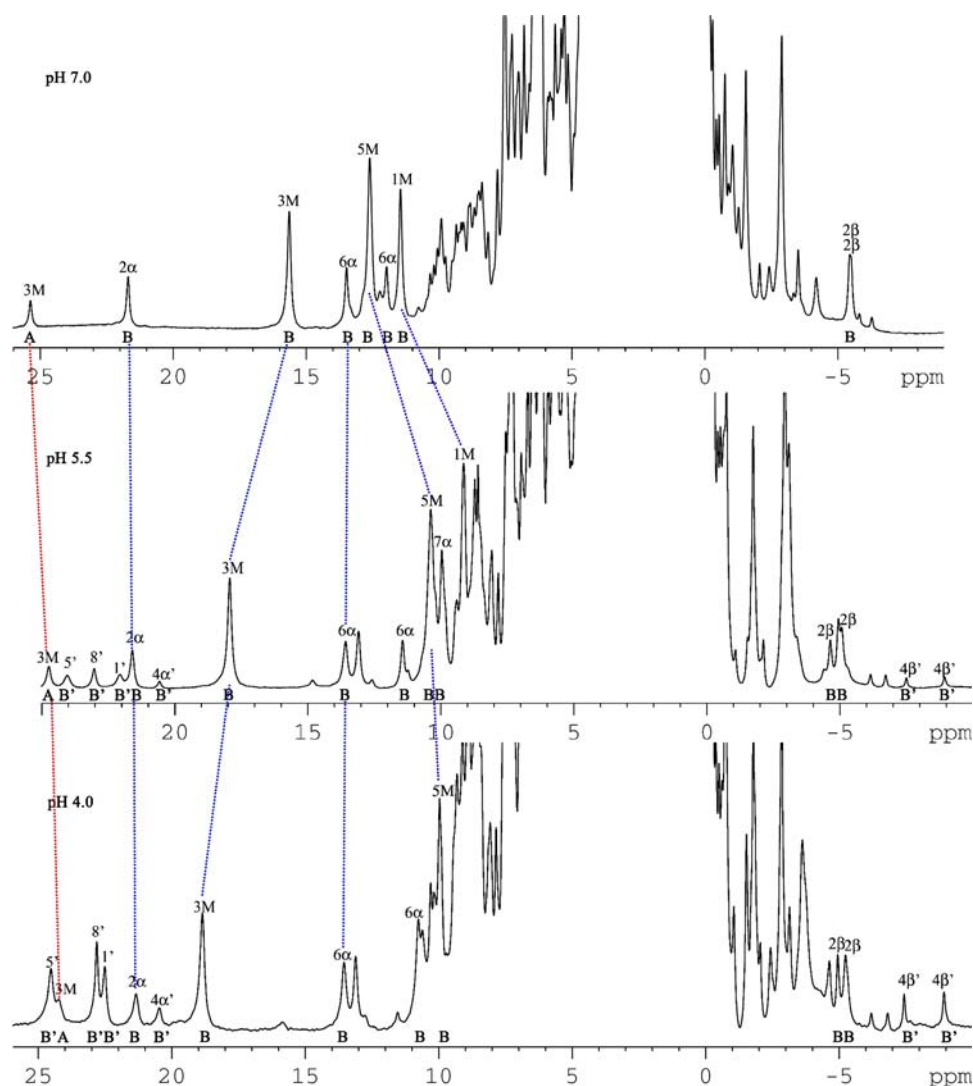
## Results

### NMR study of the NP2–imidazole (ImH) complex at low pH

The first X-ray crystallographic study of NP2 [25] showed that at equilibrium at pH 7.5 NP2 had the heme in the **B** orientation, where the 3-methyl group (3M) is close to Ile120 and the 1-methyl group (1M) is close to Leu132 (Fig. 1). NMR studies later showed that at pH\* 7.0, both heme orientations are present, with an **A**:**B** ratio of 1:8 for the high-spin complex [16] and 1:6 for the ImH complex at equilibrium [17]. Thus, the **A** heme orientation of NP2 is not observed by X-ray crystallography [25, 26], or else only the protein with **B** heme orientation crystallizes.

We (T. K. Shokhireva, F. Yang, and F. A. Walker, unpublished results) have identified NOESY cross peaks between the resonances of the **B** heme isomer (Fig. 1) discussed below and relevant protein residue protons (including Ile120 δ1 with 3M, Ile120 γ2 with 4-vinyl alpha (4Vα); Leu122 δ1,δ2 with 5-methyl group (5M) and 6α;

**Fig. 2** 1D  $^1\text{H}$  NMR spectra of the hyperfine-shifted resonances of NP2–ImH at pH\* 7.0 (*top*), pH\* 5.5 (*middle*), and pH\* 4.0 (*bottom*), recorded at 25 °C at 600 MHz. Lines showing the variation in chemical shift of heme resonances of **A** (red lines) and **B** (blue lines) are displayed



Leu132  $\delta 1, \delta 2$  and Tyr38  $\beta$  with 1M; Leu132  $\delta 1, \delta 2$ , and Ser40  $\beta$  with 2-vinyl alpha (2V $\alpha$ ), Scheme S1, all of which vary in distance from 3.8 to 4.9 Å from carbon to carbon, and approximately 2.8 to 3.9 Å from proton to proton). These nuclear Overhauser effect (NOE) cross peaks confirm the heme seating for the **B** heme orientation as being the same as observed in the crystal structure, PDB file 1EUO [25], and are consistent with the distances measured from the heme substituents to the above-mentioned protein side chain atoms, and the expected pseudocontact shifts.

In this work we studied the NP2–ImH complex at pH\* 5.5 and 4.0. As can be seen in Fig. 2, besides the major **B** orientation and minor **A** orientation, the 1D  $^1\text{H}$  NMR spectrum at pH\* 5.5 exhibits an extra set of three hyperfine-shifted resonances between 24 and 22 ppm which increased remarkably in intensity upon lowering the pH\* to 4.0. Peaks were assigned from the pH\* 5.5 [39] and the pH\* 4.0 WEFT-NOESY spectra (Fig. 3) and from the pH\* 5.5 [39] and pH\* 4.0  $^1\text{H}\{^{13}\text{C}\}$  HMQC spectra (Fig. S1).

The HMQC spectra will be discussed in more detail at the end of this section for the ligand complexes of wt NP2. The  $^1\text{H}$  and  $^{13}\text{C}$  chemical shifts at both pH values are listed in Table S1.

In 1998 Shokhirev and Walker [14] showed that the methyl and *meso*-H resonances of low-spin ferriheme proteins are strongly affected by the orientation of the plane of one or possibly both axial ligands, because the orientation of that plane determines the nodal plane orientation of the  $3e(\pi)$  orbital that is involved in spin delocalization from low-spin Fe(III) by porphyrin to Fe  $\pi$  donation, and the angular dependence of the electron–nuclear dipolar (pseudocontact) contribution to the isotropic shifts. Thus, as the planar axial ligand is rotated to a certain angle in a particular ferriheme protein, so also is the nodal plane of the  $3e(\pi)$  orbital rotated by simple rehybridization of the two Hückel orbitals, combined with the change in the angle of the pseudocontact contribution [41, 42]. This concept was shown to apply to a large number of



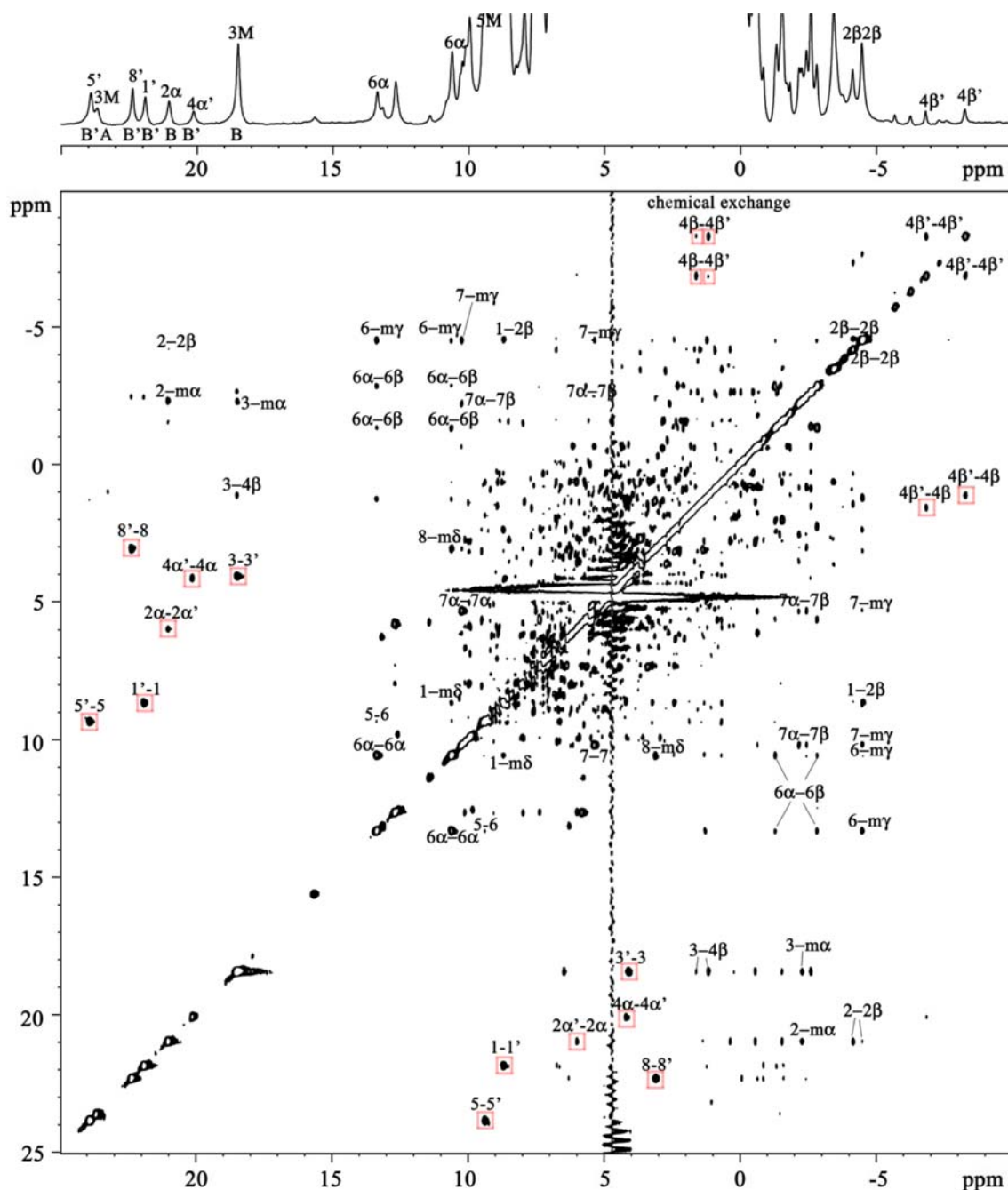


**Fig. 3** 1D and WEFT-NOESY/EXSY NMR spectra of NP2-ImH in D<sub>2</sub>O, buffered with 30 mM Na<sub>2</sub>DPO<sub>4</sub>/acetic-*d*<sub>4</sub> acid (pH\* 4.0), recorded at 33 °C and 600 MHz. There are both chemical exchange cross peaks between B' and B (red boxed), and NOESY cross peaks for B

ferriheme proteins [14] and for many more [15–19, 43–46] since that original publication. The program Shift Patterns [47] was developed for plotting methyl chemical shifts as a function of the ligand plane angle in a general way that is independent of the effect of ligand donor strength (i.e., the pattern of relative spacings is used, rather than exact chemical shifts). By using this program, we are able to determine the orientation of the nodal plane of the heme  $3e(\pi)$  orbital utilized for spin delocalization if the heme

methyl order has been assigned, by using the relative spacings of the resonances. Several systems for which this program did not predict the correct relative chemical shifts, for example, *Nitrosomonas europae* cytochrome *c*-552 [48], were later shown to have an unusual heme methyl chemical shift order ( $5M > 8M > 3M > 1M$ ) and a highly compressed chemical shift range because of dynamic flipping of the Met ligand's methyl group on the NMR time-scale, which has the effect of averaging the chemical shifts

of the heme substituents for the two possible nodal plane orientations of the Met ligand [49–52].

For the major **B** heme orientation of NP2, the order of heme methyl chemical shifts is the same from pH\* 7.0 to 4.0, 3M > 5M > 1M > 8M. From the angle plot (Fig. S2) [14, 47], because it only concerns the relative shift order instead of the numerical value, we can see that although the chemical shifts of the heme methyl change quite a bit, the effective ligand nodal plane angle varies by only a few degrees, in the range of 150–154°. That is to say, the heme methyl chemical shifts change rapidly with the small changes in axial ligand orientation over this range of angles.

Chemical exchange was observed in the NOESY/EXSY spectra at pH\* 5.5 and 4.0 between the additional signals and the 5M, 1M, 8M, and 3M resonances of the **B** orientation, thus showing that these resonances are caused by an additional species with **B** heme orientation, which we have called **B'**. The methyl resonances of **B'** are easily assigned from the chemical exchange cross peaks between **B'** and **B** from the NOESY/EXSY spectrum (Fig. 3). In contrast to the methyl resonance order 3M > 5M > 1M > 8M obtained for **B**, **B'** exhibits the order 5M > 8M > 1M > 3M at both pH\* 5.5 and pH\* 4.0. The effective ligand angle of each orientation has been determined and is listed in Table S1, from which we can see that the effective nodal plane angle of **B'** (approximately 42°) is about 109° different from that of **B** (approximately 151°). Since the proximal His imidazole plane orientation is about 135° from the heme axis defined by the line connecting N<sub>II</sub> and N<sub>IV</sub> [25, 26], it is obvious that the effective nodal plane angle obtained from the angle plot is dominated by the exogenous ligand ImH for NP2, as was observed previously at pH\* 7.0 [17]. Thus, the ImH plane in isomer **B** is nearly parallel (a difference in angle of approximately 16°) to the His57 imidazole plane, while in isomer **B'** the ImH plane is nearly perpendicular to the His imidazole plane (a difference of approximately 93°). Thus, for simplicity, we can describe the two isomers as having parallel (**B**) and perpendicular (**B'**) ImH plane orientation. It should be clear to the reader that **A** and **B** refer to the orientation of the endogenous heme *b* when it is inserted into the  $\beta$ -barrel of the NP cavity (Fig. 1), whereas **B** as compared with **B'** refers to the orientation of the exogenous ImH ligand plane for the **B** heme orientation, as will be discussed in more detail below.

Because the His57 imidazole plane has the same orientation in all structures of NP2 determined thus far (135 ± 1° from the above-mentioned heme axis) [25, 26], the derived perpendicular nodal plane angle must describe the distal, exogenous ImH orientation. Although a perpendicular orientation of the ImH ligand of NP2–ImH was not observed in our previous study of wt NP2 at pH\* 7.0

[17], the **B'** orientation was seen for the symmetrical heme complex, NP2sym–NMeIm [20], and for the protohemin NP2 Leu to Val mutants at pH\* 7.0: NP2(L122V)–ImH, NP2(L132V)–ImH, and NP2(L122V, L132V)–ImH [11]. Both Leu122 and Leu132 point from the  $\beta$ -strands above the heme pocket toward the distal side of the heme (Fig. 1), and at the time of publication of that work [11] it was believed that the perpendicular ImH orientation was permitted by the shorter Val side chain, which was able to create enough space in the distal pocket to allow ImH ligand rotation. We now understand that the reason for the existence of this perpendicular ImH orientation is the presence of a minor ruffled conformation of the heme, which cannot accommodate the parallel ImH ligand, but can allow binding of ImH in the perpendicular orientation; dissociation and rebinding of ImH are thus required in the exchange reaction.

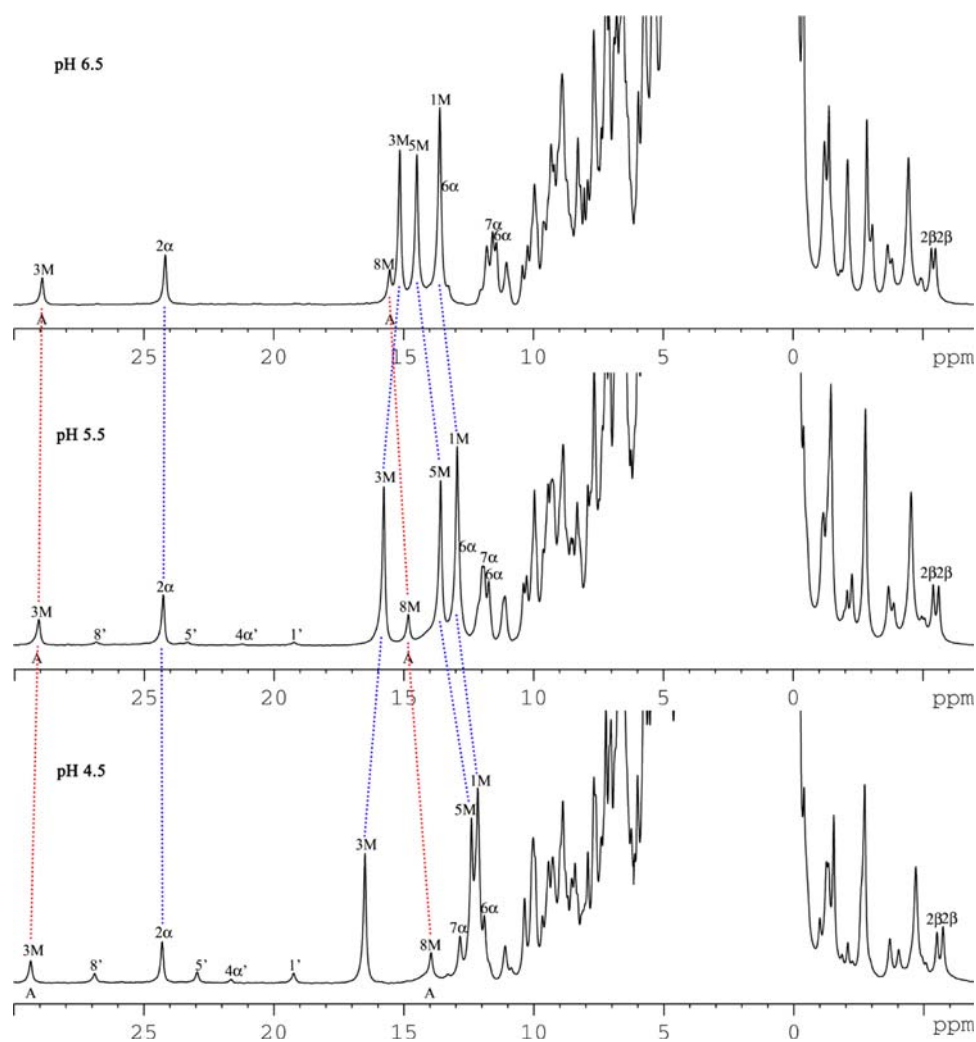
By measuring the cross peak and diagonal peak intensities, we can calculate the rate constants and equilibrium constant of interchange between **B'** and **B** using the program Two Site Exchange of NMR Lines developed in this laboratory [53]. From the results of this calculation, shown in Table 1, the equilibrium constant  $K_{\text{eq}}$  for the reaction  $\text{B}' \rightleftharpoons \text{B}$  at pH\* 5.5 is smaller than that at pH\* 4.0. This is also easily seen from the 1D <sup>1</sup>H NMR spectra (Fig. 2), which show that the peaks from **B'** at pH\* 4.0 are relatively more intense than are those at pH\* 5.5. The NOESY/EXSY spectra at different temperatures and different mixing times show that as the temperature decreases, the **B'** orientation is more favored. In other words, at low temperature the ImH ligand has more tendency to be perpendicular to the His57 imidazole plane than at room temperature. The data in Table 1 also show that different mixing times in the EXSY experiments give the same rate constant, and thus confirm that both the rate constants and the equilibrium constants are independent of mixing time.

**Table 1** Chemical exchange rate constants of NP2–ImH **B'** and **B** ligand orientation isomers measured at low pH by EXSY experiments and calculated using the program Two Site Exchange of NMR Lines [53]

$\text{B}' \rightleftharpoons \text{B}$	pH* 5.5, mix40, 33 °C	pH* 4.0, mix40, 33 °C	pH* 4.0, mix25, 33 °C	pH* 4.0, mix40, 25 °C
$k_f$ (s <sup>-1</sup> )	8.0	6.7	6.6	1.3
$k_r$ (s <sup>-1</sup> )	1.0	1.9	2.0	0.7
$K_{\text{eq}} = k_f/k_r$	8.0	3.4	3.3	2.0

*mix40* mixing time 40 ms, *mix25* mixing time 25 ms

**Fig. 4** 1D  $^1\text{H}$  NMR spectra of the hyperfine-shifted resonances of NP2–Hm at pH\* 6.5 (top), pH\* 5.5 (middle), and pH\* 4.5 (bottom), recorded at 35 °C at 600 MHz. Lines showing the variation in chemical shift of heme resonances of **A** (red lines) and **B** (blue lines) are displayed



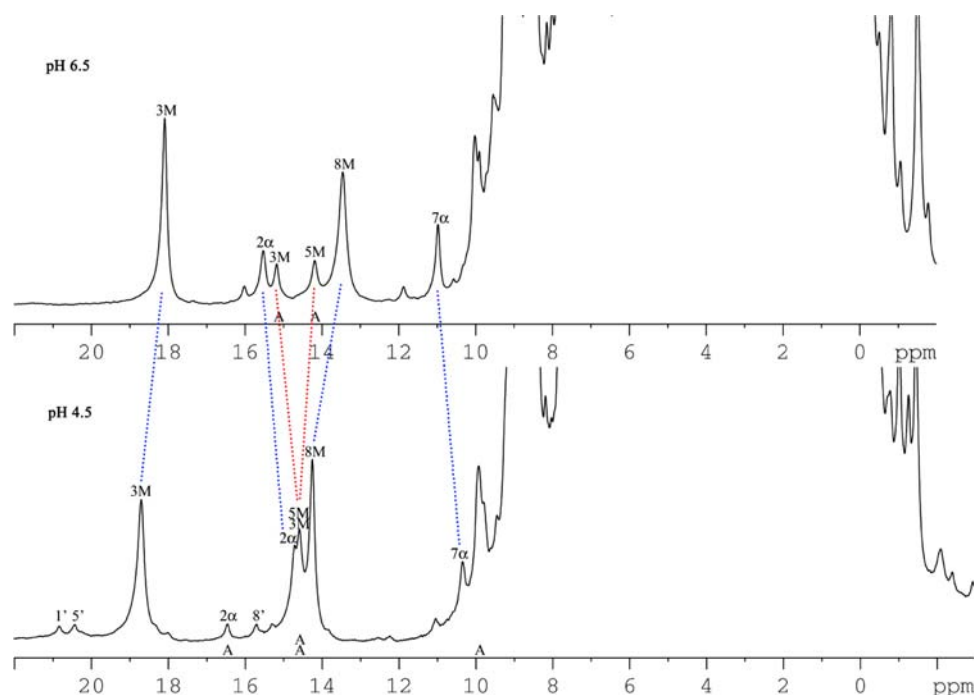
#### NMR study of the NP2–Hm complex at low pH

The NMR spectra of NP2–Hm have been studied by NMR spectroscopy at three different pH\* values (6.5, 5.5, 4.5). Representative 1D  $^1\text{H}$  spectra are shown in Fig. 4. The assignments at each pH\* value are derived from WEFT-NOESY and  $^1\text{H}\{^{13}\text{C}\}$  HMQC spectra (Figs. S3–S8), and are summarized in Table S2. At pH\* 7.0, the methyl order of the major **B** orientation is  $5\text{M} > 3\text{M} > 1\text{M} > 8\text{M}$ , and the effective ligand nodal plane orientation is  $159\text{--}160^\circ$  [17]. At pH\* 6.5, the chemical shifts of 3M and 5M change slightly from the values observed at pH\* 7.0, which leads to a change in the methyl resonance order, as listed in Table S2. The major **B** orientation at pH\* 6.5 is  $3\text{M} > 5\text{M} > 1\text{M} > 8\text{M}$ , with 3M, 5M, and 1M very close in chemical shift, but 8M is far from the other three and falls in the diamagnetic region. From the angle plot (Fig. S2) [14, 47], it can be seen that the effective ligand nodal plane orientation is  $156\text{--}157^\circ$ . Thus, although the methyl resonance order changes over this half unit of pH\*,

the effective ligand nodal plane actually decreases by only about  $3^\circ$ . And from pH\* 6.5 to 4.5, although the effective nodal plane angle decreases slightly, the methyl order for the major **B** orientation remains the same,  $3\text{M} > 5\text{M} > 1\text{M} > 8\text{M}$ .

The **A**:**B** ratio for NP2–Hm was previously reported to be 1:4 at pH\* 7.0 [17], but we find it to be 1:6 at pH\* 6.5 at equilibrium. This ratio changes only slightly, from 1:6 to 1:5, when the pH\* is lowered from 6.5 to 4.5. Later in this work we report that the **A** heme orientation increases at lower pH for NP2(V24E), but for wt NP2 the increase in **A** heme orientation was hardly noticeable. And as we have seen for the NP2–ImH complex, although the fraction of NP2–Hm with **A** heme orientation remains nearly constant, the **B**' orientation becomes more abundant as the pH drops, as is clearly shown by spectra at three pH values (Fig. 4). However, the intensity of the **B**' resonances was not sufficient to permit measurement of the rates of interchange between **B** and **B**'. From the assignment and angle plot, at both pH\* 5.5 and pH\* 4.5, the effective ligand nodal planes

**Fig. 5** 1D  $^1\text{H}$  NMR spectra of the hyperfine-shifted resonances of NP2–CN at pH\* 6.5 (*top*) and pH\* 4.5 (*bottom*), recorded at 35 °C at 500 or 600 MHz. Lines showing the variation in chemical shift of heme resonances of **A** (*red lines*) and **B** (*blue lines*) are displayed



of **B** and **B'** differ by about  $106^\circ$ , which means that as for the ImH ligand, the exogenous Hm imidazole plane has two approximately perpendicular binding modes.

#### NMR study of the NP2–CN complex at low pH

We investigated the NP2–CN complex at three different pH values, pH\* 6.5, 5.5, and 4.5. 1D  $^1\text{H}$  NMR spectra at pH\* 6.5 and 4.5 are shown in Fig. 5; WEFT-NOESY and  $^1\text{H}\{^{13}\text{C}\}$  HMQC spectra are shown in Figs. S9–S13. All assignments are listed in Table S3. Since  $\text{CN}^-$  is cylindrical, an exogenous ligand plane cannot be discussed in this case. However, as shown previously [17], the non-planarity of the heme still creates a ruffling nodal plane  $\alpha$  for isomer **A** of around  $157$ – $159^\circ$ , and for isomer **B** of around  $108$ – $112^\circ$ . In contrast, for isomer **B'** this nodal plane  $\alpha$  is around  $19^\circ$ . The methyl order for the **A** isomer is characterized by 3M having a chemical shift similar to that of 5M, and 1M having a chemical shift similar to that of 8M. The methyl order for the **B** isomer is  $3\text{M} > 8\text{M} > 1\text{M} > 5\text{M}$  at all three pH values, as we have seen for NP–CN complexes at pH\* 7.0 [17]. The fact that 1M has a larger chemical shift than 5M was previously explained by the large degree of ruffling of the heme and somewhat off-axis binding of the cyanide [17]. The methyl order for **B'** is  $1\text{M} > 5\text{M} > 8\text{M} > 3\text{M}$ . All methyl orders for **A**, **B**, and **B'** isomers are different from those of the ImH and Hm complexes.

The  $\text{p}K_a$  of HCN is 9.31 [54], and there is thus strong competition between  $\text{H}^+$  and the heme Fe(III) center for the cyanide anion at low pH. Not surprisingly, Fe(III)

competes very well, since  $K_{\text{eq}}$  for  $\text{CN}^-$  binding to NP2 at pH 7.5 is estimated to be approximately  $10^{12} \text{ M}^{-1}$ . Thus, as the pH\* was lowered to 5.5 and 4.5, the NMR resonances of the high-spin heme complex began to appear. The intensity of the high-spin resonances decreased upon increasing the concentration of NaCN at the desired pH\*, while that of the low-spin resonances increased concomitantly. The highest total concentration of NaCN used was 2 mM at pH\* 4.5. 2D NMR experiments on NP2 samples containing different  $\text{CN}^-$  concentrations up to that level showed that the residual high-spin complex is not in chemical exchange with the low-spin complex on the NMR timescale. Therefore, its presence does not affect the assignment of the low-spin resonances. If a smaller spectral window appropriate for the low-spin complex is used, with digital filtering in the acquisition parameters, the high-spin resonances from outside the spectral window are not folded or aliased. The **A**:**B** ratio for the cyanide complex was 1:6 at pH\* 6.5, and the **A** heme isomer decreased in relative abundance at lower pH\*. Whether this was a result of preferential loss of cyanide from the **A** isomer to form the high-spin complex was not determined.

As for the case of the ImH and Hm complexes, resonances from a **B'** species are observed as the pH\* is lowered. Although they are very weak in the 1D spectra, the **B'**–**B** exchange cross peaks for the methyl resonances are relatively strong in the NOESY/EXSY spectra. And by comparing the 1D spectra at pH\* 6.5 and 4.5 (Fig. 5), we see that the **B'** methyl peaks are relatively stronger at pH\* 4.5; thus, the trend is the same as seen for the ImH and Hm



complexes. Since cyanide is a cylindrical anion and has no ligand plane, the **B'** isomer does not arise from distal ligand rotation, but from dynamic changes in heme symmetry, as concluded previously [17]. It is already known that the NP2–CN complex is very ruffled (PDB file 2HYS), and as concluded previously [17] the **B'** species is a different ruffled form, with different orientation of the ruffling ridges. Although not observed in the solid state, protein dynamics in solution at ambient temperatures allow the minor ruffled form to occur transiently on the NMR timescale.

$^{13}\text{C}$  chemical shifts and the contribution of  $^1\text{H}\{^{13}\text{C}\}$  HMQC spectra to the assignment of the heme substituent resonances

The  $^1\text{H}\{^{13}\text{C}\}$  HMQC spectra of all of the above-mentioned ligand complexes were recorded as a function of  $\text{pH}^*$ . The  $^1\text{H}$  and  $^{13}\text{C}$  chemical shifts are reported in Tables S1–S3, as are those of the V24E mutant complexes discussed below. We have reported the natural-abundance  $^{13}\text{C}$  HMQC spectra of low-spin NP complexes since 2003 [17] because we find these spectra very helpful in identifying and confirming the  $^1\text{H}$  chemical shifts of heme and nearby protein substituents whose resonances are not resolved outside the protein resonance envelope. Using the information obtained from the HMQC spectra, we have been able to assign most, if not all, of the heme substituent resonances of the protein complexes of this and previous studies. For example, in Figs. S4, S6, and S8, the  $^1\text{H}\{^{13}\text{C}\}$  HMQC spectra of NP2–Hm at  $\text{pH}^*$  6.5, 5.5, and 4.5, respectively, the  $^1\text{H}$ ,  $^{13}\text{C}$  cross peaks of all heme substituents except for  $4\text{V}\alpha$ , and the *meso* cross peaks are clearly observed for the **B** heme isomer, and are fairly easy to assign because of their unique  $^1\text{H}$ ,  $^{13}\text{C}$  shifts. These unique shifts are a result of a combination of the contact, pseudocontact, and diamagnetic contributions to the chemical shifts of both nuclei [55], which shift these cross peaks well outside the normal ranges observed for the two nuclei in diamagnetic compounds, and thus make them easy to recognize and assign.

The  $\beta$ -vinyl,  $\alpha$ -propionate, and  $\beta$ -propionate C–H cross peaks can be spotted because pairs of protons have cross peaks to the same carbon.  $^1\text{H}$  resonances of the  $2\alpha$ ,  $2\beta$ ,  $4\alpha$ , and  $4\beta$ -vinyls are confirmed by their NOESY cross peaks, as are also the  $6\alpha$ ,  $6\beta$ ,  $7\alpha$ , and  $7\beta$ -propionate resonances. Other  $\text{CH}_2$  groups that are easily recognized are those of His57  $\beta$ - $\text{CH}_2$  ( $^{13}\text{C}$  chemical shift +17.7 ppm,  $^1\text{H}$  chemical shifts +12.7 and +5.8 ppm for the **B** heme orientation of wt NP2–ImH at  $\text{pH}^*$  5.5 (Fig. S1 in [39], Table S1) and  $^{13}\text{C}$  chemical shift +19.0 ppm,  $^1\text{H}$  chemical shifts +12.9 and +6.2 ppm for the **A** heme orientation of NP2(V24E)–ImH at  $\text{pH}^*$  5.5 (Fig. S3 in [39], Table S4)) and for the Hm complexes of both wt NP2 and NP2(V24E), where the His57  $\beta$   $^{13}\text{C}$  shifts are

very similar to those of the ImH complexes, and in addition, the cross peaks from the Hm  $\beta$ - $\text{CH}_2$  group (adjacent to the imidazole ring) are also observed ( $^{13}\text{C}$  chemical shift +18.7 ppm,  $^1\text{H}$  chemical shifts +9.0 and +9.4 ppm for the **B** orientation of wt NP2–Hm at  $\text{pH}^*$  6.5 (Fig. S4, Table S2), and  $^{13}\text{C}$  chemical shift 20.5 ppm,  $^1\text{H}$  chemical shifts +9.1 and +8.7 ppm for the **A** heme orientation of NP2(V24E)–Hm at  $\text{pH}^*$  7.0 (Fig. S21, Table S5)). The  $^1\text{H}$  His57  $\beta$ - $\text{CH}_2$  chemical shifts are confirmed by the NOESY spectra (T. K. Shokhireva, F. Yang, and F. A. Walker, unpublished results). Additional  $^1\text{H}$ ,  $^{13}\text{C}$  cross peaks from protein methyls of Ile120, Leu122 and Leu132, which are close to the heme, are also seen, with  $^{13}\text{C}$  chemical shifts of 10–30 ppm and  $^1\text{H}$  chemical shifts of 0 to –5 ppm (T. K. Shokhireva, F. Yang, and F. A. Walker, unpublished results). And as presented in more detail in “Discussion,” there is also a useful correlation between  $^1\text{H}$  and  $^{13}\text{C}$  shifts of the heme methyls that helps in the assignment of the heme methyl resonances and the electronic ground state of the ferriheme center. The contributions to the contact and pseudocontact shifts of heme substituents have been discussed in detail elsewhere [55].

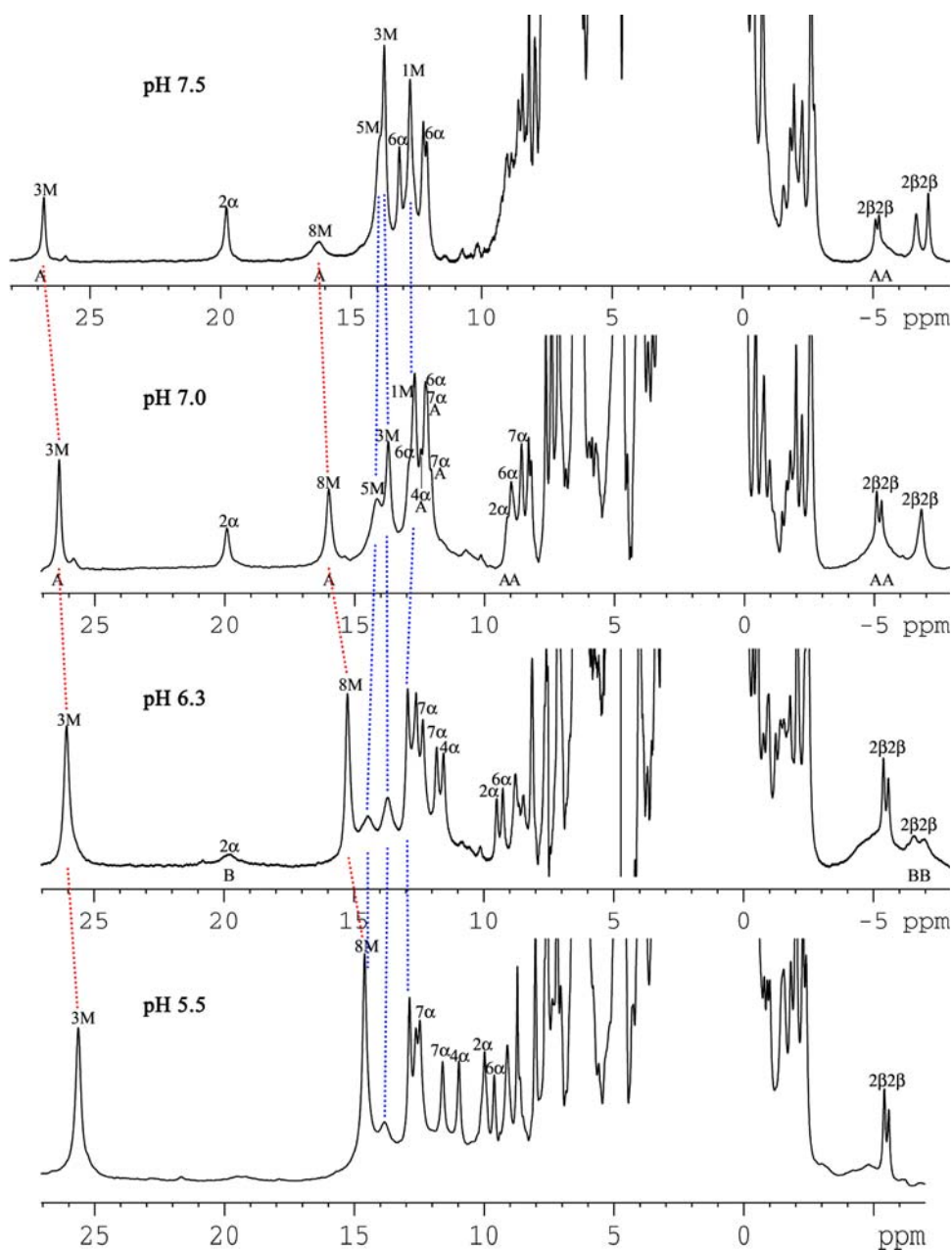
With regard to the minor **A** isomer, the heme methyl  $^1\text{H}$ ,  $^{13}\text{C}$  cross peaks, except for that of  $3\text{M}$ , are also observed. The  $^1\text{H}$ ,  $^{13}\text{C}$  cross peak for the most hyperfine-shifted methyl resonance is not usually observed because it is broader than the other three methyl resonances, as expected from its larger  $^1\text{H}$  chemical shift and thus larger expected spin density on its  $\beta$ -pyrrole carbon [14, 55]. In addition, when chemical exchange is involved, as for the wt NP2–ImH complex  $^1\text{H}\{^{13}\text{C}\}$  HMQC spectrum shown in Fig. S1, not all heme substituent cross peaks are observed, even for the major **B** isomer ( $6\alpha$ ,  $7\alpha$ ,  $2\alpha$ , and  $4\alpha$  are not observed). For wt NP2–CN the  $^1\text{H}$ ,  $^{13}\text{C}$  cross peaks for all heme substituents except the *meso*-CH are observed, as shown in Figs. S10 and S12. His57  $\beta$ - $\text{CH}_2$  cross peaks are also not seen.

To observe these  $^1\text{H}$ ,  $^{13}\text{C}$  cross peaks in the HMQC spectrum of a low-spin Fe(III) heme protein requires at least a 1 mM concentration (2 mM is preferable) of ferriheme protein at  $^{13}\text{C}$  natural abundance, and requires an experiment time of approximately 24 h. Any modern NMR spectrometer equipped with an inverse ( $^1\text{H}$  observe)  $^{13}\text{C}$  probe can be used, and 500 MHz as the  $^1\text{H}$  Larmor frequency is certainly sufficient for all systems that we have investigated. All of the  $^1\text{H}\{^{13}\text{C}\}$  HMQC spectra presented in the electronic supplementary material were recorded at 500 MHz.

NMR study of the NP2(V24E)–ImH complex as a function of pH

We now turn to the results obtained for the low-spin complexes of the V24E mutant of NP2, which was

**Fig. 6** 1D  $^1\text{H}$  NMR spectra of the hyperfine-shifted resonances of NP2(V24E)–ImH at pH\* 7.5, 7.0, 6.3, and 5.5 (from top to bottom), recorded at 35 °C at 600 MHz. Lines showing the variation in chemical shift of heme resonances of **A** (red lines) and **B** (blue lines) are displayed



prepared as a potential model of the ligand complexes of NP7. The NP2(V24E)–ImH complex has been studied at various temperatures and pH values; the 1D  $^1\text{H}$  NMR spectra at pH\* 7.5, 7.0, 6.3, and 5.5 are shown in Fig. 6. At pH\* values lower than 5.5, the resonances become very broad, and are thus not shown and were not studied in detail. 2D WEFT-NOESY and  $^1\text{H}\{^{13}\text{C}\}$  HMQC spectra were obtained at all of these pH\* values, with those obtained at low pH\* (5.5) having been presented previously [39]. Those obtained at pH\* 6.3, 7.0, and 7.5 are shown in Figs. S14–S19. Together, these 2D spectra allow us to completely assign the heme resonances and to follow their pH dependence over the entire pH\* range 5.5–7.5. All

$^1\text{H}$  and  $^{13}\text{C}$  assignments are summarized in Table S4. The  $^1\text{H}$ ,  $^{13}\text{C}$  heme substituent cross peaks were best resolved in the pH\* 7.0  $^1\text{H}\{^{13}\text{C}\}$  HMQC spectrum (Fig. S17), but in that spectrum  $2\alpha(\text{B})$  and  $5\text{M}(\text{B})$  were not observed; fewer cross peaks were observed at pH\* 6.3 (Fig. S15) and 7.5 (Fig. S19) because of a chemical exchange process that affects mainly **A** resonances at higher pH and **B** resonances at lower pH, as discussed further in the next two paragraphs.

When the pH\* was increased from 5.5 to 7.5, the  $^1\text{H}$  resonances from isomer **B** became sharper and more intense (Fig. 6). At pH\* 5.5, the **A** isomer heme resonances were dominant, with an **A**:**B** of approximately 10:1, but at

pH\* 7.5, the **A**:**B** ratio changed dramatically to 1:3. Such a large change of the **A**:**B** ratio was not observed for the wt NP2–ImH complex, and thus the pH-dependent **A**:**B** ratio change must be related to the introduction of Glu24. The change in the **A**:**B** ratio on going from wt NP2–ImH to NP2(V24E)–ImH at pH\* 7.5 reflects a change in the equilibrium constant, for  $\mathbf{A} \rightleftharpoons \mathbf{B}$ ,  $K_{\text{eq}} = 6$ ,  $\Delta G = -5.6$  kJ/mol, for wt NP2–ImH and  $K_{\text{eq}} = 3$ ,  $\Delta G = -2.8$  kJ/mol, for NP2(V24E)–ImH, a  $\Delta G$  difference of 2.8 kJ/mol. However, at pH\* 5.5 wt NP2–ImH has a similar  $K_{\text{eq}}$ , approximately 5,  $\Delta G \sim -4.1$  kJ/mol, while NP2(V24E)–ImH has  $K_{\text{eq}} \sim 0.1$ ,  $\Delta G \sim 5.9$  kJ/mol, a difference in  $\Delta G$  of 8.7 kJ/mol, from favoring the **B** isomer at high pH to strongly favoring the **A** isomer at low pH. However, this  $\Delta G$  difference does not address the most important consideration, that of the overall stability of the heme-bound proteins. While our impression is that NP2(V24E) binds heme much more weakly than does wt NP2, we have not as yet measured the equilibrium constant for heme binding to wt NP2 and its V24E mutant. The rate of **A**:**B** equilibration appears to be rapid enough that no variation in the **A**:**B** ratio has been observed with time following addition of ImH (or Hm or  $\text{CN}^-$ ). The estimated pH\* where the concentrations of **A** and **B** are equal is about 6.5, which is an estimate of the  $\text{p}K_{\text{a}}$  of this Glu24 carboxyl.

The **A** heme orientation becomes strongly stabilized by low pH, with  $K_{\text{eq}} \sim 0.1$ ,  $\Delta G \sim 5.9$  kJ/mol. However, the linewidth dependences of the **A** and **B** heme resonances are opposite to each other, in that the **A** heme resonances are broad at high pH and sharp at low pH, while the **B** heme resonances are sharp at high pH and broad at low pH. For example, the 8M resonance of isomer **A** is very broad at pH\* 7.5, but it becomes very sharp by pH\* 6.3, while the 5M resonance of isomer **B** is very sharp at pH\* 7.5, and is almost overlapped with that of 3M, but it becomes very broad by pH\* 6.3 and 5.5 (Fig. 6). This broadening prevented the observation of NOESY cross peaks of the broad resonances in the 2D spectra, and also the observation of cross peaks in the  $^1\text{H}\{^{13}\text{C}\}$  HMQC spectrum. But since the chemical shift of 5M is always expected to be larger than that of 1M (except for the  $\text{CN}^-$  complex), we assigned the broad peak at 14.2 ppm at pH\* 7.0 to 5M. The broadening of the **B** heme methyl resonances may be due to the unstable heme seating of the **B** isomer, but it is likely that two effects are involved, one that stabilizes the **A** orientation at low pH and another that stabilizes the **B** orientation at high pH.

At all pH\* values, the nodal plane angle remains nearly unchanged at approximately  $110^\circ$  for **A** and approximately  $160^\circ$  for **B**, although there are very small shifts of the **A** resonances to lower chemical shift and the **B** resonances to higher chemical shift as the pH\* is raised. The heme methyl order remains the same:  $3\text{M} > 8\text{M} > 5\text{M} > 1\text{M}$  for

**A** and  $5\text{M} > 3\text{M} > 1\text{M} > 8\text{M}$  for **B**. This order is different from that of NP2–ImH ( $3\text{M} > 5\text{M}$ ), and can be explained by an approximately  $10^\circ$  increase in the effective nodal plane angle for the ImH complex of **B** (and decrease for **A**) as compared with wt NP2. Note also that no **B'** peaks are observed for NP2(V24E)–ImH, probably because Glu24 crowds the heme enough that no change in the ruffling distortion is possible. However, because of the extreme broadening of the resonances for **B** at low pH\*, we cannot rule out the existence of a second ImH plane orientation.

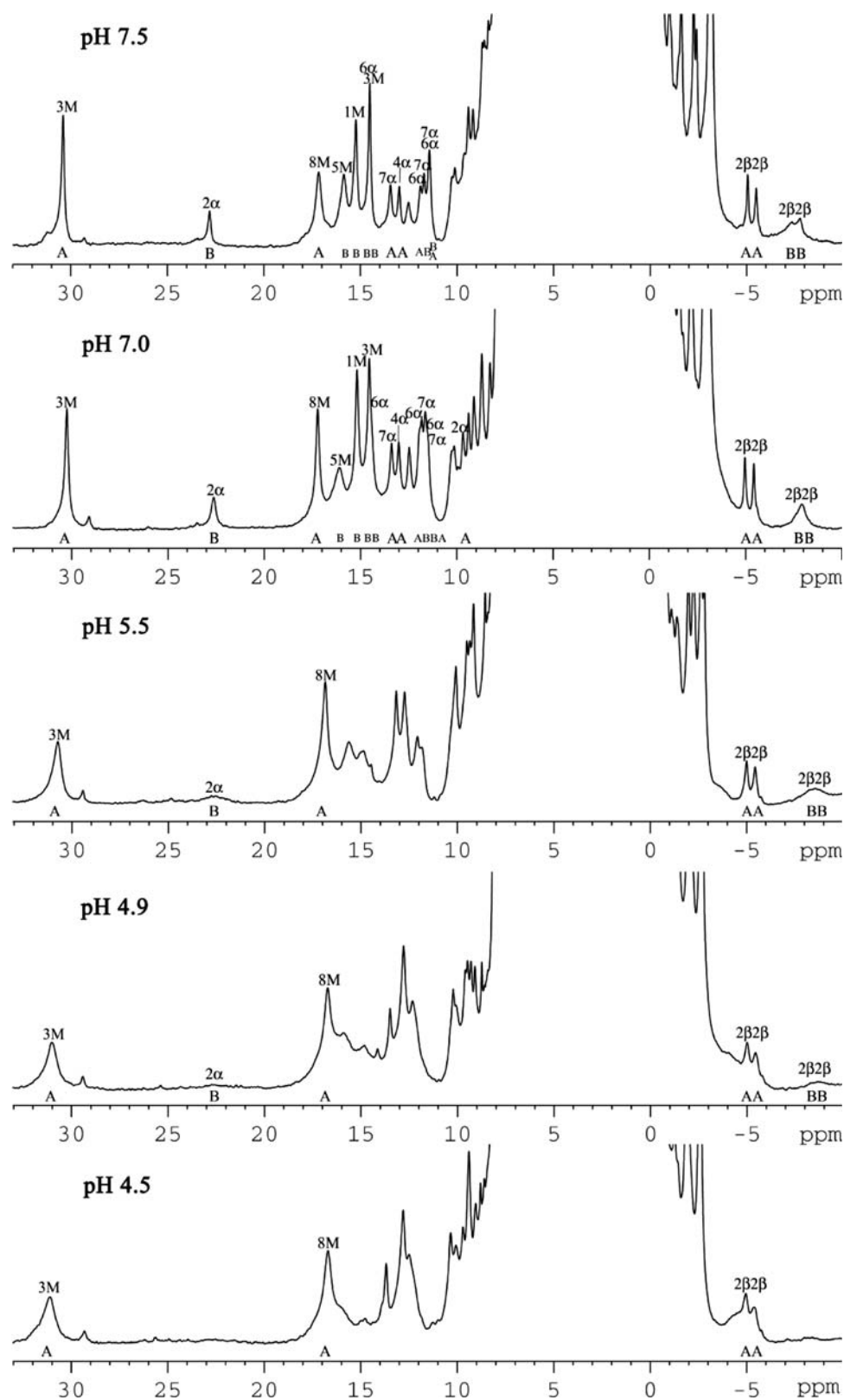
#### NMR study of the NP2(V24E)–Hm complex as a function of pH

The 1D  $^1\text{H}$  spectrum of NP2(V24E)–Hm (approximately 1 mM at pH\* 7.0) is shown in Fig. 7. 2D WEFT-NOESY and  $^1\text{H}\{^{13}\text{C}\}$  HMQC spectra (Figs. S20, S21, respectively) at 35 °C were recorded to facilitate the assignment of all heme resonances; the  $^1\text{H}$  and  $^{13}\text{C}$  chemical shifts are listed in Table S5. At this pH\*, both **A** and **B** heme orientations are observed, with the **A** isomer slightly more abundant than the **B** isomer (ratio 1:0.84, compared with 1:6 for the wt NP2–Hm complex). Thus, the equilibrium constants for  $\mathbf{A} \rightleftharpoons \mathbf{B}$  are  $K_{\text{eq}} = 6$  for wt NP2–Hm and  $K_{\text{eq}} = 0.84$  for NP2(V24E)–Hm, indicating a  $\Delta G$  difference of 6 kJ/mol between the wild type and the mutant that favors the **A** orientation. This change in the **A**:**B** ratio showed that the Val to Glu mutation strongly affects the heme orientation preference in the pocket.

At pH\* 7.0, the methyl order of the **A** isomer is  $3\text{M} > 8\text{M} > 5\text{M} > 1\text{M}$ , which is the same as for the wt NP2–Hm complex and the NP2(V24E)–ImH complex, with very similar nodal plane angle at about  $107^\circ$ . But the methyl order of the **B** isomer is  $5\text{M} > 1\text{M} > 3\text{M} > 8\text{M}$ , which is different from those of the NP2–ImH ( $3\text{M} > 5\text{M} > 1\text{M} > 8\text{M}$ ), NP2–Hm ( $3\text{M} > 5\text{M} > 1\text{M} > 8\text{M}$ ), and NP2(V24E)–ImH ( $5\text{M} > 3\text{M} > 1\text{M} > 8\text{M}$ ) complexes. This represents a change in effective nodal plane angle from  $154^\circ$  (NP2–ImH), to  $157^\circ$  (NP2–Hm),  $160^\circ$  (NP2(V24E)–ImH), and  $163^\circ$  (NP2(V24E)–Hm). Thus, both the mutation and the identity of the distal ligand affect the ligand plane orientation in the same direction: the larger the ligand and the larger the side chain of residue 24, the larger the nodal plane angle is for the heme ligand of the **B** heme isomer.

When this sample was titrated to lower pH\* (5.5, 4.9, and 4.5), the resonances became very broad at various temperatures from 15 to 35 °C (Fig. 7). Concomitantly, the 2D spectra were not well enough resolved for full assignment. The breadth of the resonances created by low pH must relate specifically to the Hm ligand, since we did not see it for the NP2(V24E)–ImH and NP2(V24E)–CN complexes. But similarly to the NP2(V24E)–ImH complex, as the pH was

**Fig. 7** 1D  $^1\text{H}$  NMR spectra of the hyperfine-shifted resonances of the NP2(V24E)-Hm at pH\* 7.5, 7.0, 5.5, 4.9, and 4.5 (from top to bottom), recorded at 35 °C at 500 or 600 MHz



lowered, the resonances of the **B** isomer decreased in intensity, and the **A** orientation was the main one observable at pH\* 4.5. Just to confirm the reproducibility of the

changes observed, this sample was then titrated to pH\* 7.5, which showed that the 1D spectrum was very similar to that at pH\* 7.0, and the resonances were sharp and well



resolved. The **A**:**B** ratio at equilibrium became 1:0.9. The assignment of the peaks outside the diamagnetic protein envelope was achieved by simple comparison with the pH\* 7.0 spectra.

#### NMR study of the NP2(V24E)–CN complex as a function of pH

The NP2(V24E)–CN complex was studied at various temperatures and pH values from pH\* 7.0, then pH\* 5.5, and following the low-pH measurements the sample was titrated back to pH\* 7.7. From this pH titration, changes in the **A**:**B** ratio were clearly reproducible at a given pH\*. 2D WEFT-NOESY and  $^1\text{H}\{^{13}\text{C}\}$  HMQC spectra were recorded at pH\* 5.5 (Figs. S22–S24), 7.0 (Figs. S25, S26), and 7.7 (Figs. S27, S28) to assign the heme resonances. The greatest number of  $^1\text{H},^{13}\text{C}$  cross peaks were observed in the pH\* 5.5  $^1\text{H}\{^{13}\text{C}\}$  HMQC spectrum (Fig. S24), where the resonances were the sharpest; only the **A** heme isomer resonances were clearly resolved at this pH\*. All  $^1\text{H}$  and  $^{13}\text{C}$  assignments and **A**:**B** ratios are summarized in Table S6.

At all pH values, the methyl order for **A** is always  $3\text{M} > 5\text{M} > 1\text{M} > 8\text{M}$ , and for **B** is always  $3\text{M} > 8\text{M} > 1\text{M} > 5\text{M}$ , which is similar to that of the wt NP2–CN complex at higher pH. These orders are very different from those of the ImH and Hm complexes. As we have seen for other cyanide complexes [17, 20], the **B** isomer of NP2(V24E)–CN has reversed 1M and 5M order.

At pH\* 5.5, the signals from the **A** heme orientation are dominant. Full assignment was accomplished at both 35 and 25 °C. At pH\* 7.0 and 7.7, both **A** and **B** are observable; only some resonances were assigned, because they are broader compared with those observed at pH\* 5.5. In Fig. S25 we can see the two sets of cross peaks between the 3M and 2V $\alpha$  protons, one from **A** and one from **B**. As the pH increases, the **B** orientation becomes more favored relative to the **A** orientation, as we have seen for other NP2(V24E) complexes. This indicates that the pH-dependent **A**:**B** ratio of NP2(V24E) and the  $\Delta G$  for heme orientation are controlled by the negative charge/steric effect caused by the Val to Glu mutation, which changes dramatically with the protonation state of Glu24.

## Discussion

Up to this point, the low-spin NP NMR spectra have been reported almost exclusively at pH\* 7.0 [11, 15, 17–20]. However, in addition to their “pH of action” at approximately 7.4 in the extracellular space in the tissues, it is

important to consider the pH of the NP-containing *R. prolixus* saliva; this pH is between 5 and 6 [40]. Thus, when the insect pumps its saliva into the host’s tissues, the resulting major pH change induces large structural and functional alterations in the NPs [9, 29–31] (R. E. Berry, F. Yang, T. K. Shokhireva, H. Zhang, W. R. Montfort, and F. A. Walker, unpublished results). Therefore, the NMR spectroscopic investigation of NP2 at low pH\*, reported herein, is an important extension of our understanding of these proteins, in particular in view of the unprecedentedly detailed insights with respect to the orientation and dynamics of the heme cofactor inside the protein obtained by NMR spectroscopy compared with other spectroscopic methods. We have found that in distinction to wt NP2 at pH\* 7.0 [11, 15, 17–20], at lower pH this protein exhibits chemical exchange between two ruffled conformations of the heme, as was observed previously for NP1, NP3, and NP4 at pH\* 7.0 [17]; thus, the behavior of NP2 may now be seen to be the same as that of the other three major NPs, when the entire pH range of importance to the biology of these proteins is considered. This study has also increased our understanding of the structural and NMR spectroscopic properties of the ferriheme surroundings of NP7 through study of its model NP2(V24E) as a function of pH\* from 5.5 to 7.5.

We have also shown that the natural-abundance  $^1\text{H}\{^{13}\text{C}\}$  HMQC spectra of the low-spin axial ligand complexes, wt NP2-L and NP2(V24E)-L, are very helpful in assigning the heme and some nearby protein side chain resonances that have  $^1\text{H}$  chemical shifts which place them within the diamagnetic protein envelope. This is because the combination of their  $^1\text{H}$  and  $^{13}\text{C}$  chemical shifts [55] yields unique  $^1\text{H},^{13}\text{C}$  cross peaks that are easily recognized and assigned. However, if chemical exchange exists between two different species, the  $^1\text{H},^{13}\text{C}$  cross peaks may not be observed. When they are observed, the ferriheme methyl cross peaks present a fairly linear correlation of  $^{13}\text{C}$  and  $^1\text{H}$  chemical shifts, as can be seen in Figs. S4, S6, S8, S10, S12, S15, S17, S19, S21, S24, and S28. For the ImH and Hm ligand complexes of this study, the slope of this line is typically 1.7–2.3, which appears to be a hallmark of the  $(d_{xy})^2(d_{xz},d_{yz})^3$  electron configuration of the ferriheme center. In contrast, for the cyanide complexes the slope is typically 0.8–1.4, a hallmark of the  $(d_{xz},d_{yz})^4(d_{xy})^1$  electron configuration of the ferriheme center. This correlation appears to hold for a wide range of other low-spin ferriheme proteins (F. Yang and F. A. Walker, unpublished results).

The  $^1\text{H}$  NMR spectra of the ImH and Hm complexes of the major **B** isomer of wt NP2 both show changes in the chemical shifts of the heme methyls as the pH\* is lowered from 7.0 to 5.5 and in the case of the ImH complex to pH\* 4.0, and both complexes also show chemical exchange with

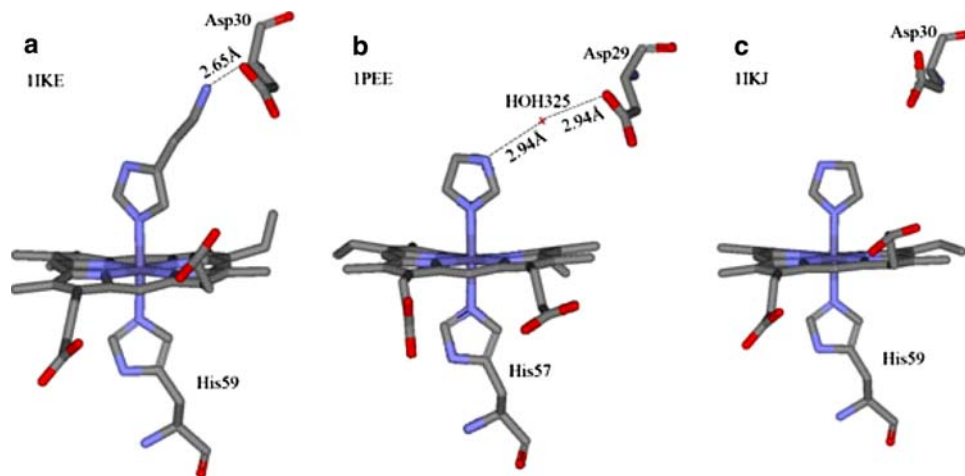
a new species that is not observed at pH\* 7.0, as shown in Figs. 2 and 4 for the ImH and Hm complexes, respectively. For both complexes the chemical shift of 3M increases, while the chemical shifts of 5M and 1M decrease as the pH is lowered, with the magnitude of the changes being much larger for the ImH complex than for the Hm complex. These changes in chemical shift suggest a change in the orientation of the exogenous ligand, a decrease in the angle with decreasing pH from approximately 154° [15] to approximately 151° and 150° at pH\* 5.5 and 4.0, respectively (Table S1). These angles represent a nearly parallel orientation ( $\Delta\varphi \sim 19\text{--}15^\circ$ ) of the imidazole planes of ImH and the protein-provided His57, the latter of which has been shown by X-ray crystallography to be almost perfectly aligned along the *meso*- $\beta$ , *meso*- $\delta$  axis of the heme, at an angle of  $135 \pm 1^\circ$  [25, 26]. For the Hm complex, the imidazole plane angle is fairly similar (nodal plane  $\varphi \sim 157^\circ$ ) and the trends in chemical shift changes as the pH\* is lowered are the same, but the magnitude of the changes in chemical shifts and imidazole plane angle are much smaller, a change from 157° at pH\* 7.0 to 156° at pH\* 4.5. As found previously [15], the exogenous ligand contributes more to the effective nodal plane that defines the heme methyl pattern [14] than does the protein-provided His57. The A:B heme rotational isomer ratio is 1:6 for both the ImH and Hm complexes at pH\* 7.0, and it does not change markedly as the pH\* is lowered to 5.5 and 4.0. This ratio defines the equilibrium constant for the reaction  $A \rightleftharpoons B$  as  $K_{\text{eq}} = 6$ , which represents a free-energy stabilization,  $\Delta G = -4.5$  kJ/mol, for the B heme isomer.

As for the B' species, the ImH complex has a much larger fraction of B' at lower pH\* than does the Hm complex, and it is possible to measure the rate of exchange between B' and B in that case (Table 1), while for the Hm complex the B' resonances are observed (Fig. 4), but they are so low in intensity that it is not possible to estimate the rate constants. The reason for the lower intensity of B' for

Hm than for ImH is likely because of the larger size of Hm, which may impede formation of the perpendicular ligand complex. The existence of species B' is readily shown to result from a second possible orientation of the ImH or Hm imidazole plane, one that is approximately perpendicular to the His57 ligand plane ( $\varphi = 42\text{--}40^\circ$  and  $51\text{--}52^\circ$ , respectively;  $\Delta\varphi = 93\text{--}95^\circ$  and  $84\text{--}83^\circ$ , respectively).

Both the small change in exogenous ligand plane orientation and the existence of a B' species as the pH is decreased *might* be explained by the protonation of Asp29 (or Asp30 in the numbering system of NP1 and NP4) at low pH\*. Crystal structures of the Hm complexes of NP1 [24] and NP4 [29] show a strong hydrogen bond between the  $\text{--NH}_3^+$  side chain of Hm and the carboxylate of Asp30, as shown in Fig. 8a. The structure of NP1–Hm was solved at pH 7.5 (PDB file 1NP1) [24], while that of NP4–Hm was solved at pH 5.6 (PDB file 1IKE) [29], and an unpublished structure of NP2(D1A)–Hm has been solved at pH 7.5 (A. Weichsel, R. E. Berry, H. Zhang, F. A. Walker, and W. R. Montfort, unpublished results), but the N(Hm)–O(Asp) distances are similar for all three (2.73, 2.65, and 2.75 Å, respectively). Although we estimated the  $\text{p}K_{\text{a}}$  of Asp29 of NP2–D1A(NO) to be 5.4 and that of Asp30 of NP4(NO) to be 5.5 [12], there is no guarantee that the  $\text{p}K_{\text{a}}$  values of these carboxyl side chains will be the same for the Hm complexes. Nevertheless, it is very likely that both Asp29 of NP2 and Asp30 of NP1 and NP4 are protonated at pH\* 4.0 for both ligand complexes. Thus, the shift in imidazole plane orientation, as estimated from the heme methyl  $^1\text{H}$  shift pattern, at least for the Hm complex, could be due to the loss of the hydrogen bond between the  $\text{--NH}_3^+$  side chain of Hm and the protonated carboxyl of Asp29 at this low pH. However, the change in orientation of the Hm imidazole plane is extremely small over the pH range 6.5–5.5, and the large size of Hm should prevent it from rotating freely in the crowded distal pocket, with other protein side chains present. (However, at pH\* 4.5 the  $^1\text{H}$

**Fig. 8** Representation of the nitrophorin–ligand interaction in crystal structures of NP2 and nitrophorin 4 (NP4). **a** Hydrogen bond between Hm  $\text{NH}_3^+$  and Asp30 of the NP4–Hm complex [29] [Protein Data Bank (PDB) file 1IKE]. **b** Water-mediated hydrogen bond between ImH NH and Asp29 of the wild-type NP2–ImH complex [25] (PDB file 1PEE). **c** No hydrogen bond between ImH NH and Asp30 of the NP4–ImH complex [29] (PDB file 1IKJ)



NMR spectrum of NP2–Hm is extremely broad, which might suggest loss of the hydrogen-bond anchor to the Asp29 carboxyl.) With regard to the NP2–ImH complex, the ImH N–H proton hydrogen-bonds to a water molecule that in turn hydrogen-bonds to the carboxyl of Asp29: The N–O(water) and O(water)–O(carboxyl) distances are both longer, at 2.94 Å (Fig. 8b). In comparison, NP4–ImH shows no hydrogen-bonding interaction between the ImH N–H and Asp30 (Fig. 8c). This suggests that the hydrogen bonds observed for NP2–ImH that involve the water molecule are likely very weak and may not be present in solution. Furthermore, even at pH\* 7.0, the *N*-methyl imidazole (NMeIm) complex of the symmetrical heme version of NP2 shows a second ligand orientation, with chemical exchange between the major and minor forms which differ in orientation by about 60° [20]; no hydrogen-bonding interaction is possible for NMeIm as an exogenous ligand. Thus, we conclude that it is unlikely that hydrogen-bonding interactions with Asp29 are responsible for the relatively small changes in ImH plane orientation for the major **B** species of the NP2–ImH and NP2–Hm complexes. More likely, the changes in chemical shifts of the heme methyl resonances, which represent relatively small changes in imidazole plane orientation, are related to changes in the size and/or shape of the heme distal pocket, as discussed below.

The presence of a second **B** heme axial ligand plane orientation for the ImH and Hm complexes (the **B'** species) of NP2 at low pH and the chemical exchange between them are not unique; NP2sym–NMeIm shows a major and minor ligand orientation species (**B** and **B'**) and chemical exchange between them, which was believed to be due to the symmetrical heme being less distorted than protohemin (which thus allows the exogenous ligand to have a second ligand orientation about 60° different from the major one) [20]. In addition, NP2(L122V)–ImH, NP2(L132V)–ImH, and NP2(L122V,L132V)–ImH also show minor ImH orientations with chemical exchange between the major and minor orientations (which was believed to be due to the increased space in the distal pocket which could allow the ImH to rotate by about 110°) [11]. The crystal structure of NP2(L122V,L132V)–ImH was later shown to have only this alternate, perpendicular ImH orientation in the solid state, although the angle differs from that estimated in solution from the <sup>1</sup>H shifts of the heme methyls by about 20° (PDB file 1PM1) [26]. In addition, we also observed chemical exchange that we attributed to changes in heme seating of about 10° for the symmetrical heme complexes of the NPs in the high-spin form [19]. We now understand that most of these types of chemical exchange (except heme seating changes) are related to heme ruffling dynamics [20], which may involve only heme nonplanar dynamics, or, because of the slow

timescale involved, may also contain contributions from slow motions of the protein backbone that stabilize the minor ruffling isomer. In any case, there are clearly a number of types of dynamic processes that occur for the heme center of the NPs that cannot be captured by X-ray crystallography. NMR spectroscopy provides a fast, direct, and effective means for gathering dynamic structural information on these interesting proteins.

As mentioned in “Results” (and as shown in Figs. 5, S11, S13), NP2–CN also exhibits a **B'** species, although the distal ligand in this case is cylindrical rather than planar. The symmetrical heme complexes of NP1–CN, NP3–CN, and NP4–CN at pH\* 7.0 were previously shown to have strong chemical exchange cross peaks in the NOESY/EXSY spectra, while NP2sym–CN at pH\* 7.0 showed no evidence of chemical exchange [20]. It is now clear, on the basis of this work, that at lower pH\* values (5.5 and 4.5) protohemin-containing NP2–CN also exhibits chemical exchange cross peaks (Figs. S11, S13), and thus it is likely that NP2sym–CN would also have shown chemical exchange cross peaks in the NOESY/EXSY spectra at lower pH\* values. As concluded in the symmetrical heme study [20], the chemical exchange observed for the cyanide complex of NP2 at low pH\* in the present study must also be between two different ruffling distortions of the highly ruffled protohemin ring ( $\alpha = 108\text{--}109^\circ$  and approximately  $19^\circ$  for **B** and **B'**, respectively;  $\Delta\alpha = 89\text{--}90^\circ$ ). If this is the case for the cyanide complex of NP2, then, as concluded earlier for the symmetrical heme NP–ligand complexes [20], it is likely that the chemical exchange observed for the ImH and Hm complexes is also a result of two different ruffling distortions of the heme ring. This suggests that the ImH and Hm ligands may lose their ability to bind to Fe as the “major” ruffling ridge rotates with changes in protein conformation, and as a result of this rotation the planar distal ligand dissociates from the heme pocket and reenters with an orientation that better matches the “minor” ruffling distortion. Thus, in line with the conclusions for the symmetrical heme complexes of NP1, NP2, NP3, and NP4 [20], we conclude that the heme is constantly changing its ruffling distortion between two extreme possibilities, one “major” and one “minor,” whose rate of interchange and relative abundance are determined by relatively slow protein conformational changes, and the ImH or Hm bond to Fe likely breaks and the ligand leaves and reenters the distal pocket in a different orientation; the difference in angle for these two orientations is about 110° for ImH and about 106° for Hm.

We now return to the question of why no chemical exchange is observed for NP2–ImH, NP2–Hm, and NP2–CN at pH\* 7.0, although there clearly is chemical exchange for all three ligand complexes at lower pH\* values, and why a pH change affects the heme ruffling and zero ruffling

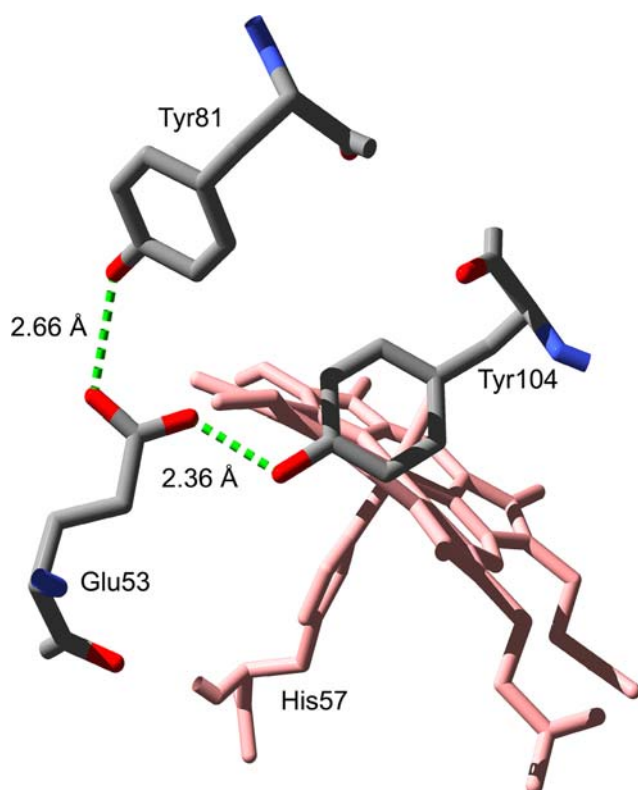


**Fig. 9** View of the hydrogen-bonding network that involves Glu53 carboxylate, Tyr81–OH and Tyr104–OH groups. At pH values lower than the  $pK_a$  of Glu53 (estimated as 5.8 [12]) these hydrogen bonds will be weakened by protonation of Glu53. This will allow these three residues to move independently, which may create chemical exchange between several conformers

line  $\alpha$ . It appears that there are other important pH-dependent effects, apart from or in addition to a potential hydrogen bond between Asp29 and the planar axial ligand, that exist in NP2 and its complexes. One possibility may be effects related to Glu53, for which the estimated  $pK_a$  for the NO complex of NP2(D1A) is about 5.8 [12]. Glu53 acts as hydrogen-bond acceptor from both Tyr104 and Tyr81 in all structures of NP2 [Tyr104(OH)–(OC)Glu53 = 2.36 Å; Tyr81(OH)–(OC)Glu53 = 2.66 Å] [25, 26], as shown in Fig. 9, and similar hydrogen-bond acceptance by Glu55 of NP1 [24] and NP4 [27–31] from Tyr105 (but not Tyr82, which points away from Glu55, toward the surface of the protein) is evident in the structures of those proteins. There are no structures of any of the NPs at pH values lower than 5.6, and none for NP2 at pH lower than 6.5, but it is tempting to postulate that if Glu53 of NP2 were protonated, hydrogen-bond donation from Tyr104 to Glu53 could not occur. Since Tyr104 is one of the “belt” residues whose primary role is believed to be to “shield” the heme from the protein backbone and hold it in its ruffled conformation, the pH-dependent hydrogen-bond formation and breakage might lead to motion of the side chain of Tyr104

that could increase the likelihood of the interchange of different ruffling distortions of the heme at low pH values.

Overall, the present study shows that wt NP2 strongly maintains the **B** heme orientation, even at the pH of the *R. prolixus* saliva (approximately 5–6) [40]. Thus, this is the first extensive investigation on the NP–cofactor interaction that reflects the pH condition at which the NPs are produced and stored in vivo. The stability of the **A**:**B** ratio of wt NP2 over the  $pH^*$  range 4.5–7.0 is not trivial, as is shown by the strong pH dependence of the **A**:**B** ratio in the case of the single-residue mutant NP2(V24E). In particular, the NP2–CN complex is a structural model for the native NP2–NO complex, both of which are linear two-atom ligands. Because of the diamagnetism of the low-spin ferric nitrosyl complex, insights into the structure and conformation of the heme cannot be gained as easily as for the paramagnetic complexes. Thus, the increased stabilization of the previously predicted minor heme ruffling form **B'** of the cyanide complex [17] at low pH, and the determination of the **B'**  $\rightleftharpoons$  **B** dynamics add significantly to our picture of the slow molecular motions of the heme center in NP2.

Recently, the motion of the cofactor inside NP4 was addressed by femtosecond coherence spectroscopy, which showed low-energy (less than  $200\text{ cm}^{-1}$ ) dynamics of the heme plane [56]. However, these motions are in the time regime of picoseconds, which is the same as that of the very fast breaking and reformation of the Fe–NO bond within the heme pocket (geminate recombination) [57]. On the other hand, determination of the kinetics of NO release from the NPs revealed NO release rates in a time regime similar to that of the **B'**  $\rightleftharpoons$  **B** exchange (Table 1), for instance, for wt NP2 the NO  $k_{\text{off}}$  is  $0.12\text{ s}^{-1}$  at pH 8.0 [9]. The difference between the rate of Fe–NO bond breakage and the release of the NO molecule is attributed to numerous collisions of the NO molecule with the protein matrix in the crowded distal pocket, and subsequent multiple rebinding events before the barrier of the protein envelope is overcome [57, 58]. A similar situation can be expected for the larger ImH and Hm release rates and subsequent rebinding to the **B'** form, except that the rate should be slower. However, at  $pH^* \geq 6.5$  in the case of ImH as a ligand, **B'** was not detected, and it is expected that the decreasing size of  $k_r$  (see Table 1) continues with increasing pH, so **B'** may not be visible by NMR spectroscopy at high pH.

Whereas for NP2 low-pH NMR spectra have not previously been reported, for NP7 high-pH NMR spectra could not be obtained because of aggregation of the protein [38, 39]. Therefore, the mutant NP2(V24E) was created to address the particular role of the remarkably unique Glu27 in NP7, and NMR spectra at  $pH^* 5.5$  had been recorded previously, and exhibited features comparable to those of wild-type NP7 with respect to the existence of only the **A**



heme orientation [39]. In view of the stability of the **A**:**B** ratio in NP2 with change in pH on the one hand, and the appearance of the **B'** species with decreasing pH on the other, similar investigations were performed with NP2(V24E) using the same set of ligand complexes for comparison. Although wt NP2–ImH, wt NP2–Hm, and wt NP2–CN all have similar **A**:**B** heme orientation ratios, the **A**:**B** heme orientation ratios of NP2(V24E)–ImH, NP2(V24E)–Hm, and NP2(V24E)–CN differ significantly from each other at a given pH, and the ratios change markedly as the pH is changed. For example, at pH\* 7.0 the **A**:**B** heme ratios are 1:2, 1:0.84, and 1:1.1, respectively for the three ligand complexes. At lower pH\* values these ratios change significantly, and at pH\* 5.5 for ImH mainly **A** was observed (little or no **B** was detectable) and for CN<sup>−</sup> the **A**:**B** ratio was 3:1. (For the Hm complex at pH\* 5.5, the spectra were too broad, and thus the ratio could not be determined.) Thus the exogenous ligand has a much larger effect on the **A**:**B** ratio than is the case for wt NP2. This appears to be because for NP2(V24E) the distal pocket is more crowded as a result of the mutation, and thus the heme is more sensitive to any exogenous ligand. Consequently, each different ligand creates a different pathway for stabilization of the heme. For instance, at pH\* 7.0, the **A**:**B** ratio of the ImH complex changes from 1:6 to 1:2 upon the V24E mutation, a  $\Delta G$  difference of 2.8 kJ/mol. This change must be the result of the contribution of the steric effect of the longer side chain of Glu, because from the X-ray crystal structure of NP2–ImH (1PEE), the Val is pointing directly at the 2-vinyl group (**B** orientation), with Val24  $\gamma$ -CH<sub>3</sub>  $\leftrightarrow$  vinyl  $\beta$ -CH<sub>2</sub> distances of approximately 4 Å. For comparison, a structural model of the mutant was built based on this structure (Fig. 10), which has Glu24 substituted at this position and heme inserted in the **B** orientation. This model suggests that the longer Glu side chain would cause severe steric interference with the 2-vinyl  $\beta$ -carbon and its two protons [38]. Figure 10a shows a view from the side of the heme with His57 below, which shows that the  $\gamma$ -carbon of Glu24 contacts the heme 2-vinyl  $\beta$ -carbon. Figure 10b shows the view from above the heme with His57 behind the heme. It can easily be seen that the Glu24 side chain would be very crowded with such a close distance to the 2-vinyl  $\beta$ -CH<sub>2</sub> of the **B** heme orientation. Instead, by rotating the heme to the **A** orientation, in which 3M, a smaller substituent, is present at that position, Glu24 can nestle between the 2-vinyl and 4-vinyl groups. As mentioned above, the rate of **A**:**B** equilibration appears to be rapid enough that no variation in the **A**:**B** ratio was observed with time, following addition of an axial ligand. This suggests that heme binding to the NP2(V24E) mutant may not be as strong as to wt NP2.

In previous work the NP7(E27V)–ImH mutant NMR spectrum was reported and discussed [39]. That mutant at

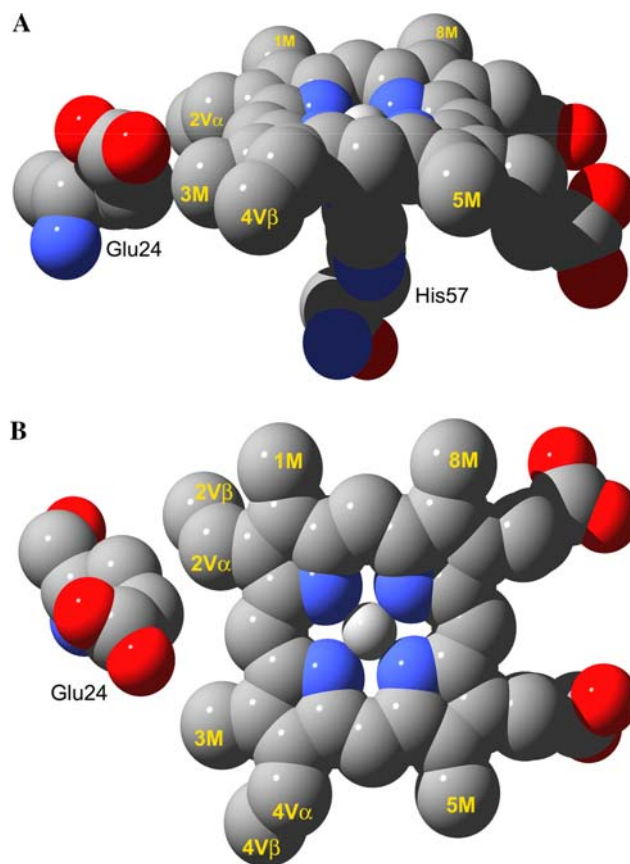


**Fig. 10** Structural model of NP2(V24E). **a** Side view of the heme *b* cofactor in the **B** orientation, which is displayed together with the His57 ligand bound to Fe, and Glu24. **b** View from above the heme cofactor and Glu24. The model was prepared by manipulation of the NP2 crystal structure, PDB file 1PEE, in Swiss-PdbViewer 4.0.1 (<http://spdbv.vital-it.ch/>) [59]. Energy minimization of the total structure using the implemented Gromos96 algorithm was performed without significant changes. Graphics were rendered with POV-Ray 3.6 (<http://www.povray.org/>)

pH\* 5.5 has an **A**:**B** heme orientation ratio of 1:3, whereas for the NP7(E27Q)–ImH complex the **A** isomer was the major form at pH 5.0 [39]. Compared with the wt NP7, the E27Q mutant does not change the predominance of the **A** isomer, while the E27V does [39]. Since Gln is structurally similar to a protonated Glu, it is easy to see why there is almost no change in the heme **A**:**B** ratio for NP7(E27Q). But Val is much shorter than Glu, which thus allows more space for the heme to become stable as the **B** heme isomer. In unpublished work we have also investigated the NP2(V24L) and NP2(V24I) mutants and the ImH ligand complex of the latter. We found that NP2(V24L) could not be fully reconstituted with hemin. Thus, it appears that Leu24 is too bulky to allow hemin binding, probably because it is unable to fold its side chain into a nonlinear rotamer, as may be assumed to be necessary from the position of Glu24 in the homology model of NP2(V24E), Fig. 10a, and thus neither **A** nor **B** heme orientation fits into the heme pocket. In contrast,

NP2(V24I)–ImH has NMR spectra at pH\* 5.5 and 35 °C (Fig. S29) and an A:B heme ratio (1:5) similar to those of wt NP2–ImH at that pH\*. We hypothesize that this is because the ethyl group of the Ile side chain is able to bend out of the way of the heme, thus allowing it to have similar bulk as the Val side chain of the wild-type protein with respect to the heme substituents. Thus, the length of the side chain and also the carboxyl/amido group, at position 24 (27 for NP7), are extremely important factors in the stabilization of the A heme orientation. Whether the strong pH dependence of the A:B ratio can be attributed to NP7 cannot be said at present because structural information on NP7 is as yet very limited. However, the insertion of Glu24 into NP2 is an impressive example of the influence of a single residue on the heme cofactor orientation, and it demonstrates the importance of Val24 for the proper functionality of wt NP2. Interestingly, unlike wt NP2, chemical exchange cross peaks of the B heme orientation, even at low pH, were not obtained for any of the three NP2(V24E) ligand complexes. This may be a consequence of the more crowded heme pocket explained above.

In conclusion, by detailed comparison of the ligand complexes of wt NP2 and NP2(V24E) as a function of pH we are able to see that the wild-type protein pocket shape favors the B orientation, and no matter what ligand is added, the heme can adapt to it without changing heme orientation. In contrast, NP2(V24E) ligand complexes favor the A orientation at lower pH\*, where Glu24 is protonated, but the B orientation at pH\* values above 7, where Glu24 is deprotonated. Since the NP proteins are stored at pH 5–6 in the salivary glands of the insect, this study has greatly increased our understanding of the properties of NP2 and NP2(V24E), as a model of NP7, at these low pH\* values. Furthermore, the study indicates the relevance of understanding the unique Glu27 residue in NP7 to the unique structural features of this protein. The characterization of any of the NPs is particularly important in order to address the still open question of the reason for the presence of so many different NPs in the saliva of *R. prolixus*. Moreover, the study exemplifies the potential of a single residue inside a protein structure to modulate the heme cofactor positioning, and is therefore generally inspiring for research on heme proteins.

**Acknowledgments** This work was supported by National Institutes of Health grant HL054826 (F.A.W.), the Chemistry Discretionary Fund (F.A.W.), a Center for Insect Sciences (CIS) Graduate Student Research Support grant (F.Y.), and the Max Planck Society (M.K.).

## References

- Ribeiro JMC, Hazzard JM, Nussenzveig RH, Champagne DE, Walker FA (1993) *Science* 260:539–541
- Champagne DE, Nussenzveig RH, Ribeiro JMC (1995) *J Biol Chem* 270:8691–8695
- Ribeiro JMC, Nussenzveig RH (1993) *FEBS Lett* 330:165–168
- Nussenzveig RH, Bentley DL, Ribeiro JMC (1995) *J Exp Biol* 198:1093–1098
- Yuda M, Hirai M, Miura K, Matsumura H, Ando K, Chinzei Y (1996) *Eur J Biochem* 242:807–812
- Walker FA (2005) *J Inorg Biochem* 99:216–236
- Ribeiro JMC, Walker FA (1994) *J Exp Med* 180:2251–2257
- Ding XD, Weichsel A, Andersen JF, Shokhireva TK, Balfour C, Pierik AJ, Averill BA, Montfort WR, Walker FA (1999) *J Am Chem Soc* 121:128–138
- Andersen JF, Ding XD, Balfour C, Shokhireva TK, Champagne DE, Walker FA, Montfort WR (2000) *Biochemistry* 39:10118–10131
- Berry RE, Ding XD, Shokhireva TK, Weichsel A, Montfort WR, Walker FA (2004) *J Biol Inorg Chem* 9:135–144
- Shokhireva TK, Berry RE, Uno E, Balfour CA, Zhang H, Walker FA (2003) *Proc Natl Acad Sci USA* 100:3778–3783
- Berry RE, Shokhirev MN, Ho AYW, Yang F, Shokhireva TK, Zhang H, Weichsel A, Montfort WR, Walker FA (2009) *J Am Chem Soc* 131:2313–2327
- Maes EM, Walker FA, Montfort WR, Czernuszewicz RS (2001) *J Am Chem Soc* 123:11664–11672
- Shokhirev NV, Walker FA (1998) *J Biol Inorg Chem* 3:581–594
- Shokhireva TK, Shokhirev NV, Walker FA (2003) *Biochemistry* 42:679–693
- Shokhireva TK, Smith KM, Berry RE, Shokhirev NV, Balfour CA, Zhang H, Walker FA (2007) *Inorg Chem* 46:170–178
- Shokhireva TK, Weichsel A, Smith KM, Berry RE, Shokhirev NV, Balfour CA, Zhang H, Montfort WR, Walker FA (2007) *Inorg Chem* 46:2041–2056
- Shokhireva TK, Berry RE, Zhang H, Shokhirev NV, Walker FA (2008) *Inorg Chim Acta* 361:925–940
- Berry RE, Shokhireva TK, Filippov I, Shokhirev MN, Zhang H, Walker FA (2007) *Biochemistry* 46:6830–6843
- Shokhireva TK, Shokhirev NV, Berry RE, Zhang H, Walker FA (2008) *J Biol Inorg Chem* 13:941–959
- Astashkin AV, Raitsimring AM, Walker FA (1999) *Chem Phys Lett* 306:9–17
- Wegner P, Benda R, Schünemann V, Trautwein AX, Berry RE, Balfour CA, Wert D, Walker FA (2002) *Hyperfine Interact* C5:253–256
- Andersen JF, Champagne DE, Weichsel A, Ribeiro JMC, Balfour CA, Dress V, Montfort WR (1997) *Biochemistry* 36:4423–4428
- Weichsel A, Andersen JF, Champagne DE, Walker FA, Montfort WR (1998) *Nat Struct Biol* 5:304–309
- Andersen JF, Montfort WR (2000) *J Biol Chem* 275:30496–30503
- Weichsel A, Berry RE, Zhang H, Walker FA, Montfort WR (1999–2002) Protein Data Bank (PDB) files available: 1PEE, 1PM1, 1T68, 2A3F, 2ACP, 2AH7, 2AL0, 2ALL, 2AMM, 2ASN, 2EU7, 2HYS, 2GTF. <http://www.rcsb.org/>
- Andersen JF, Weichsel A, Balfour CA, Champagne DE, Montfort WR (1998) *Structure* 6:1315–1327
- Weichsel A, Andersen JF, Roberts SA, Montfort WR (2000) *Nat Struct Biol* 7:551–554
- Roberts SA, Weichsel A, Qiu Y, Shelnett JA, Walker FA, Montfort WR (2001) *Biochemistry* 40:11327–11337
- Maes EM, Weichsel A, Andersen JF, Shepley D, Montfort WR (2004) *Biochemistry* 43:6679–6690
- Maes EM, Roberts SA, Weichsel A, Montfort WR (2005) *Biochemistry* 44:12690–12699
- Montfort WR, Weichsel A, Andersen JF (2000) *Biochim Biophys Acta* 1482:110–118

33. La Mar GN, Walker FA (1979) In: Dolphin D (ed) The porphyrins, vol IV. Academic Press, New York, pp 61–157
34. Walker FA (2000) In: Kadish KM, Smith KM, Guillard R (eds) The porphyrin handbook, chap. 36, vol 5. Academic Press, San Diego, pp 81–183
35. La Mar GN, Satterlee JD, De Ropp JS (2000) In: Kadish KM, Smith KM, Guillard R (eds) The porphyrin handbook, chap. 37, vol 5. Academic Press, San Diego, pp 185–298
36. Andersen JF, Gudderra NP, Francischetti IMB, Valenzuela JG, Ribeiro JMC (2004) *Biochemistry* 43:6987–6994
37. Knipp M, Zhang H, Berry RE, Walker FA (2007) *Protein Expr Purif* 54:183–191
38. Knipp M, Yang F, Berry RE, Zhang H, Shokhirev MN, Walker FA (2007) *Biochemistry* 46:13254–13268
39. Yang F, Zhang H, Knipp M (2009) *Biochemistry* 48:235–241
40. Soares AC, Carvalho-Tavares J, Gontijo NdF, dos Santos VC, Teixeira MM, Pereira MH (2006) *J Insect Physiol* 52:468–472
41. Tan H, Simonis U, Shokhirev NV, Walker FA (1994) *J Am Chem Soc* 116:5784–5790
42. Shokhirev NV, Walker FA (1998) *J Am Chem Soc* 120:981–990
43. Caignan GA, Deshmukh R, Wilks A, Zeng Y, Huang H-W, Moenne-Loccoz P, Bunce RA, Eastman MA, Rivera M (2002) *J Am Chem Soc* 124:14879–14892
44. Caignan GA, Deshmukh R, Zeng Y, Wilks A, Bunce RA, Rivera M (2003) *J Am Chem Soc* 125:11842–11852
45. Zeng Y, Deshmukh R, Caignan GA, Bunce RA, Rivera M, Wilks A (2004) *Biochemistry* 43:5222–5238
46. Deshmukh R, Zeng Y, Furci LM, Huang H, Morgan BN, Sander S, Alontaga AY, Bunce RA, Moëne-Loccoz P, Rivera M, Wilks A (2005) *Biochemistry* 44:13713–13723
47. Shokhirev NV, Walker FA (2005) Shift patterns—heme methyl shift patterns v2. <http://www.shokhirev.com/nikolai/programs/prgsciedu.html>
48. Timkovich R, Cai M, Zhang B, Arciero DM, Hooper AB (1994) *Eur J Biochem* 226:159–168
49. Zhong L, Wen X, Rabinowitz TM, Russell BS, Karan EF, Bren KL (2004) *Proc Natl Acad Sci USA* 101:8637–8642
50. Wen X, Bren KL (2005) *Biochemistry* 44:5225–5233
51. Wen X, Bren KL (2005) *Inorg Chem* 44:8587–8593
52. Wen X, Patel KM, Russell BS, Bren KL (2007) *Biochemistry* 46:2537–2544
53. Shokhirev NV, Walker FA (2000) Two site exchange of NMR lines. <http://www.shokhirev.com/nikolai/programs/prgsciedu.html>
54. Weast RC (ed) (1969) *Handbook of chemistry and physics*. The Chemical Rubber Co, Cleveland. Ed. 50, D119
55. Banci L, Bertini I, Luchinat C, Pierattelli R, Shokhirev NV, Walker FA (1998) *J Am Chem Soc* 120:8472–8479
56. Kubo M, Gruia F, Benabbas A, Barabanschikov A, Montfort WR, Maes EM, Champion PM (2008) *J Am Chem Soc* 130:9800–9811
57. Swails JM, Meng Y, Walker FA, Marti MA, Estrin DA, Roitberg AE (2009) *J Phys Chem B* 113:1192–1201
58. Nienhaus K, Maes EM, Weichsel A, Montfort WR, Nienhaus GU (2004) *J Biol Chem* 279:39401–39407
59. Guex N, Peitsch MC (1997) *Electrophoresis* 18:2714–2723